CHALMERS

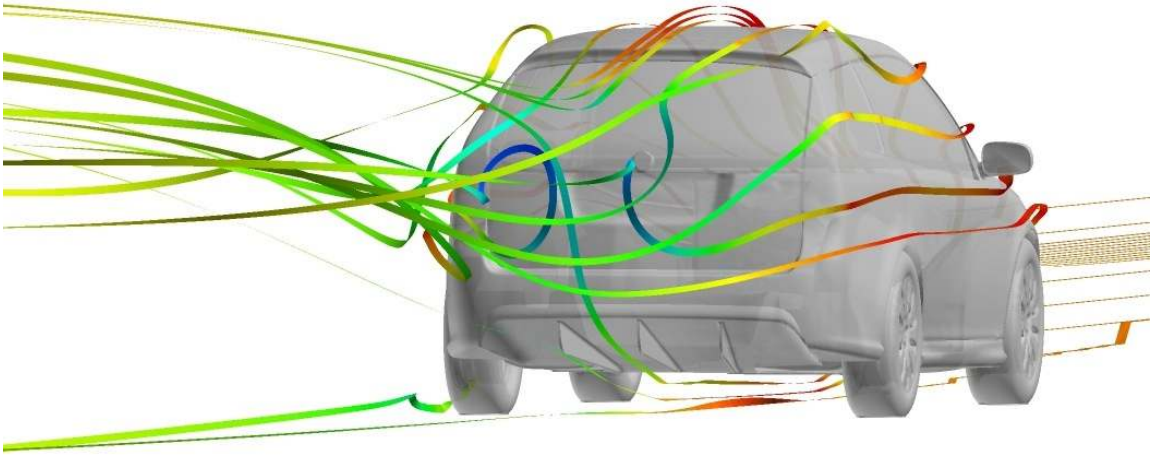

Aerodynamic analysis of drag reduction devices on the underbody for SAAB 9-3 by using CFD

Master's Thesis in Automotive Engineering

JOHAN LEVIN
RIKARD RIGDAL

Department of Applied Mechanics
Division of Vehicle Engineering and Autonomus Systems
CHALMERS UNIVERSITY OF TECHNOLOGY
Göteborg, Sweden 2011
Master's Thesis 2011:30

MASTER'S THESIS 2011:30

Aerodynamic analysis of drag reduction devices on the underbody for SAAB 9-3 by using CFD

Master's Thesis in Automotive Engineering

JOHAN LEVIN
RIKARD RIGDAL

Department of Applied Mechanics
Division of Vehicle Engineering and Autonomus Systems
CHALMERS UNIVERSITY OF TECHNOLOGY
Göteborg, Sweden 2011

Aerodynamic analysis of drag reduction devices on the underbody for SAAB 9-3 by using CFD
JOHAN LEVIN
RIKARD RIGDAL

Master's Thesis 2011:30
ISSN 1652-8557
Department of Applied Mechanics
Division of Vehicle Engineering and Autonomus Systems
Chalmers University of Technology
SE-412 96 Göteborg
Sweden
Telephone: + 46 (0)31-772 1000

Cover:
Velocity streamlines on SAAB 9-3 Sportswagon with a diffuser

Chalmers Reproservice
Göteborg, Sweden 2011

Aerodynamic analysis of drag reduction devices on the underbody for SAAB 9-3 by using CFD
Master's Thesis in Automotive Engineering
JOHAN LEVIN
RIKARD RIGDAL
Department of Applied Mechanics
Division of Vehicle Engineering and Autonomus Systems
Chalmers University of Technology

Abstract

Environmental issues and increased fuel prices are driving forces for the automotive manufactures to develop more fuel efficient vehicles with lower emissions. Large investments are aimed at minimizing power needed for propulsion i.e. new downsized engines with new aerodynamic devices for drag reduction. For passenger cars the aerodynamic drag force is the dominating resistance force at higher velocity. The car body is often optimized for reducing the drag resistance but one region where the aerodynamic development has not reach its full potential is the design of the underbody.

To explain the aerodynamic force in a simplified manner the resisting drag originates from the pressure difference between the stagnation pressure in the front and the base pressure at the rear. By reducing the difference in pressure the drag force will be reduced hence the fuel consumption will be reduced. A device to improve the aerodynamics that is used on sports- and racing-cars is a diffuser, with lower ground clearance the diffuser generates downforce and aid the braking, cornering and acceleration. Using a diffuser on a passenger car, with higher ground clearance, will improve the pressure recovery on the underbody and the base pressure will be increased. To get an effective diffuser a flat underbody is preferred which also contributes to reducing the resisting drag force.

In this study the drag reduction effect of a diffuser with panels on the underbody have been studied on the *SAAB 9-3 Sport sedan* and the *SAAB 9-3 Sports wagon*. To measure the effect of altering the underbody *Computational Fluid Dynamics* (CFD) simulations has been performed for the analysis, i.e. no wind tunnel tests have been performed. The simulations showed that a great improvement of the aerodynamic drag force can be achieved with a flat underbody and a diffuser. It was also found that the rear-end of the vehicles has an effect of the diffusers effect, a steeper diffuser is to prefer on a rear-end with steep rear-windscreen e.g. the sedan.

Different additional aerodynamic devices and diffuser designs was simulated to find the most effective drag reduction setup, it was found that the most effective configuration consisted of a diffuser with covered rear rims. A reason for the drag reduction was found that the turbulent crossflow through the rims was prevented which was advantageous for the pressure recovery and overall streamlining of the pressure wake behind the vehicle.

This study has shown that there are still possibilities to improve the aerodynamics of vehicles, especially at the underbody. By implementing panels at the underbody and a diffuser the drag resistance can significantly be reduced and hence a lower fuel consumption.

Keyword: CFD, Diffuser, Drag reduction, Underbody, Aerodynamics, Pressure recovery, Wake balance, Steady state

Contents

List of Figures

List of Tables

Aknowledgements

This master thesis has been performed in collaboration with *SAAB Automobile AB* which gave us the opportunity to work within the area of road vehicle aerodynamics and *Computational Fluid Dynamics (CFD)*. We would like to extend a great thank a large number of people that has been supporting us during this project. First of all we would like to express our gratitude to our supervisor Jesper Marklund at *SAAB Automobile AB* for his support and expertise. We would also like to thank the vehicle aerodynamic group at *Chalmers University of Technology* a special thanks goes out to Christoffer Landström and David Söderblom for ideas, showed interest and for there expertise and support during this study. We are also grateful to Alexey Vdovin for his support on hardware issues.

A great support and source of inspiration has been provided by our examiner Professor Lennart Löfdahl at *Chalmers University of Technology* which has provided necessary resources for performing this study.

We also take the opportunity to give out a thanks the aerodynamic- and CFD-group at SAAB Automobile which has provide a great deal of support.

Göteborg June 2011
Johan Levin, Rikard Rigdal

Notations

A_f	Projected frontal area of vehicle $[m^2]$
C_d	Drag coefficient [-]
C_l	Lift coefficient [-]
C_m	Moment coefficient [-]
C_p	Pressure coefficient [-]
c_p	Specific heat capacity $[J/kg \cdot K]$
ρ	Density $[kg/m^3]$
F_A	Acceleration resistance $[N]$
F_D	Drag force $[N]$
F_G	Gravitation force $[N]$
F_L	Lift force $[N]$
F_R	Rolling resistance $[N]$
g	Gravity $[m/s^2]$
k	Coefficient of thermal conductivity $[W/K \cdot m]$
p	Static Pressure $[Pa]$
T	Temperature $[K]$
U	Freestream velocity $[m/s]$
V	Velocity $[m/s]$
μ	Static viscosity $[kg/m \cdot s]$
Φ	Viscous dissipation function [-]
y^+	Dimensionless wall distance [-]

Abberivations

CAD	Computer Aided Design
CFD	Computational Fluid Dynamics
PID	Property Identification
RANS	Reynolds Averaged Navier-Stoke
SAAB	Svenska Aeroplan Aktiebolaget

1 Introduction

In this section the background, objectives, challenges, scopes and the method can be found.

1.1 Background

In order to be a competitive passenger car manufacture a large effort must be put into reducing fuel consumption and increase the overall efficiency to meet the future demand for more fuel efficient vehicles.

A cost effective way to reduce the fuel consumption of a vehicle is to improve the aerodynamic behavior and reduce the aerodynamic drag resistance. The drag resistance of a vehicle can be derived from primarily the exterior shape.

When investigating the aerodynamics behavior of a vehicle, wind tunnel tests are often a good tool but has a high cost and often takes place late in the development process which makes it hard to make any modifications. An alternative or complement to running full-scale wind tunnel test is using simulation tools as *CFD* (Computational Fluid Dynamics) codes which enable the possibility to make modifications early in the development process.

Formula one has been at the forefront within the field of aerodynamics and it was in the racing industry the exploitation of the underbody airflow was utilized at first. It was discovered that the airflow under the vehicle was noticeably affected by the close proximity to the ground and it was at this time a large amount of development time was dedicated to researching ground effects. At first the objective was to increase the negative lift force (downforce) by accelerating the underbody airflow by reducing the cross-sectional area and creating a region of low pressure, but it was soon discovered that this under certain circumstances had a positive impact to the drag.

A famous quote during the time of introducing diffusers into racing was done by Lotus Formula 1 team in 1978:

"We have found something for nothing" (Lotus announcement about Lotus Type 78 F1 car, 1978)

This reflects the benefit with introducing diffusers which gives a gain in negative lift and a reduction in drag. In the racing of today diffusers can be found on every car, depending on it's ability to create downforce which aid the braking, cornering and acceleration. Due to the increased fuel prices and the environmental effects also the passenger car companies are looking on diffusers as an complement to reduce drag.

1.2 Objective

The main objective for this thesis is to investigate the possibility to increase the base pressure and reduce the form drag of the vehicles *SAAB 9-3 Sports wagon* and *SAAB 9-3 Sport sedan* by designing new underbody shapes. This will be carried out by using commercial CFD codes.

To increase the base pressure the exterior shape can be altered to influence the wake behind the vehicle which is a large source of drag. A popular design approach is to sweep the underbody at the rear end and create a pressure recovery zone by slowing down the airflow under the body. This can be seen as a Venturi tunnel and is referred to as a diffuser within the automotive industry.

SAAB's main goal with this thesis work is to be able to present a functional and cost effective diffuser solution that will reduce the drag resistance according to simulated results from commercial CFD code.

1.3 Challenges

- Can a diffuser reduce drag(high/low speeds)?
- How is lift affected?
- How is the underbody flow affected?
- How is cooling flow affected?
- Cost effective?

1.4 Scope

The scope of this master thesis will not include the influence of crosswind and exterior shape alterations will only be done on the underbody.

No physical test will be performed only computer simulations will be done with commercial CFD codes which does not take temperature shifting and air density variations into consideration.

The simulations will be done at a fixed velocity of *140 km/h (38.89 m/s)*, there is an agreement that CFD simulations will be performed at that particular velocity.

1.5 Method

To investigate the influence of a diffuser a reference case had to be simulated in order to measure any improvements. Since the rear end wake is depending on the upper body shape a base case had to be done for both the sedan and wagon passenger car. A complete 3D-model of the *SAAB 9-3* is provided by *SAAB Automobile* that were meshed and prepared for CFD simulations. One of the reasons for doing this investigation is to find the ruling parameters for an optimal diffuser.

A competitor analysis was performed to investigate the diffusers impact on the commercial market within passenger cars. It's was found that a tuning company, Hirsch Performance, designed diffuser suited for *SAAB*. CAD-models of the diffuser was provided through *SAAB* and was used for observation since the suspicion is that some of the current designs mainly are styling features.

The design of the diffuser is done in Catia v5 and the parameters affecting the drag, i.e. length and angle, will be different for each case. The design of the diffuser has to meet the requirements of having realistic geometry and feasible to us in a production vehicle.

A CFD simulation includes three parts:

- Pre-processing
- Solving of the equations
- Post-processing

The pre-processing will include CAD-cleaning and mesh generating. To be able to generate a surface mesh the surface of the model can't have holes and bad surface connections. The pre-processing is made in ANSA and TGrid, softwares which are commonly used in the automotive industry for CFD-simulation. To be able to describe the flow in the diffuser the governing equations has to be solved, this will be made in Fluent. In Fluent all the indata for the case will be stated, i.e. boundary conditions and turbulence model. The post-processing and the visualization is done in FieldView and Fluent.

2 Theory

In this section the theory that this investigation is based on will be presented. First a section with some general fluid mechanics theory, as well as more specific theory for flow around vehicles. Furthermore the diffuser will be explained, both as a drag reduction device and as a downforce generator. There will also be a section about CFD theory.

2.1 Fluid mechanics

Fluid dynamics describes the motion of fluid (gas & liquid) in terms of *energy*, *momentum* and *mass*. This study consists of solving the flow field around a vehicle by using a commercial CFD (*Computational fluid dynamics*) -tool. The software solves the governing equations for fluid flow for an finite number of cells in a generated grid domain.

A first approach for describing the flow field is to state the three laws of conservation and assuming incompressible and isothermal flow. By doing this assumption the density and viscosity can be seen as constant due to conditions where the velocity is below Mach number 0.3 ($Ma = 0.3 \approx 100\ [m/s]$) and the temperature is relatively low during the simulation of the flow field.

- **Conservation of mass** - equal amount of mass enters and leaves the control volume.

$$Continuity\ equation: \quad \frac{\partial u}{\partial x} + \frac{\partial v}{\partial y} + \frac{\partial w}{\partial z} = 0 \tag{1}$$

- **Conservation of linear momentum** (Newton's 2^{nd} law of motion) - relation between pressure, momentum and viscous forces. This set of formulas are referred as the incompressible *Navier-Stokes* equations which are non-linear partial differential equations.

$$\begin{aligned} \rho g_x - \frac{\partial p}{\partial x} + \mu\left(\frac{\partial^2 u}{\partial x^2} + \frac{\partial^2 u}{\partial y^2} + \frac{\partial^2 u}{\partial z^2}\right) &= \rho\frac{du}{dt} \\ \rho g_y - \frac{\partial p}{\partial y} + \mu\left(\frac{\partial^2 v}{\partial x^2} + \frac{\partial^2 v}{\partial y^2} + \frac{\partial^2 v}{\partial z^2}\right) &= \rho\frac{dv}{dt} \\ \rho g_z - \frac{\partial p}{\partial z} + \mu\left(\frac{\partial^2 w}{\partial x^2} + \frac{\partial^2 w}{\partial y^2} + \frac{\partial^2 w}{\partial z^2}\right) &= \rho\frac{dw}{dt} \end{aligned} \tag{2}$$

- **Conservation of energy** (1^{st} law of thermodynamics) - the total amount of energy within the system stays constant.

$$\rho c_p \frac{dT}{dt} = k\nabla^2 T + \Phi \tag{3}$$

$$\begin{cases} \rho = density \\ t = time \\ p = pressure \\ \mu = static\ viscosity \\ g = gravity\ constant \\ c_p = specific\ heat\ capacity \\ T = temperature \\ k = coefficient\ of\ thermal\ conductivity \\ \Phi = viscous\ dissipation\ function \end{cases} \tag{4}$$

Due to the stochastic, three-dimensional, time dependent and turbulent flow there will be fluctuations within the flow field. To handle this the *Navier-Stokes* equations (Eq.2) must be time-averaged which will be described in Section 2.4.2.

2.1.1 Flow Around a Passenger Car

A vehicle that travels on a road is exposed to different kinds of resistance, Figure 1. The total resistance force on a moving vehicle with constant velocity is the sum of the *rolling resistance*, the *gravitational resistance, acceleration resistance* and the *aerodynamic drag resistance*.[10] These resisting forces must be overcome in order to propel the vehicle forward. To express the total resistance the *equation of motion* is used, Eq. (5).

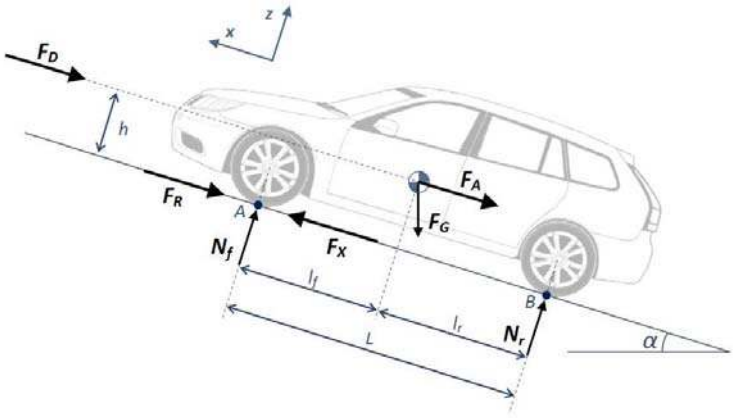

Figure 1: Resistance on a passenger car

$$F_X = F_A + F_R + F_G + F_D = ma + f_R\, mg\, cos\alpha + mg\, sin\alpha + \frac{1}{2}\rho C_D A_f U^2 \tag{5}$$

The inclination resistance is independent of the velocity and since CFD calculations are performed on flat road the inclination resistance can be neglected. During lower velocities the rolling resistance is the dominating resisting force. For velocities above *70 km/h* the aerodynamic drag will be the dominating resistance due to the fact that the drag is increasing with the square of the speed. Figure 2 shows the rolling resistance and the aerodynamic resistance as a function of the velocity, the rolling resistance slightly increase with the total resistance but can be assumed constant for velocities below *100 km/h*.

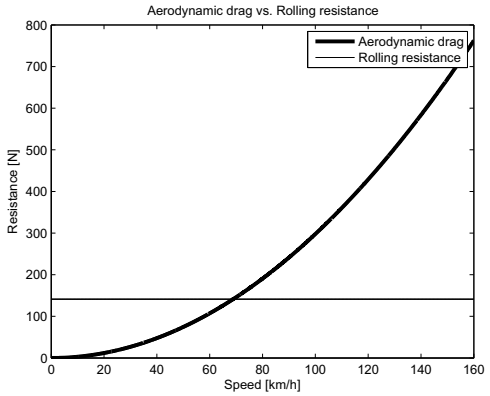

Figure 2: Aerodynamic drag and rolling resistance versus velocity

The aerodynamic drag force (F_D) can be divided into two components, *form-* and *friction force*. The form (pressure) drag acts in the direction normal to the surfaces, meanwhile the friction force is acting tangential to the surface. Due to the scale and shape of a passenger car the form drag is dominating and the vehicle can be assumed to be a bluff body. This means that a big *wake* and *vortices* will be present in the flow field.[10] The form drag is created by the pressure difference between the front and rear part of the vehicle. The friction on the surface is a source of energy loss since the air flow slows down near the surface and will eventually separate from the body. Since the pressure distribution over the body is not symmetric and the pressure on the rear will be lower then in the front, there will be a rearward directed drag force. Due to *Bernoulli's Equation*, Eq. (6), it can been seen that the high pressure peak in the front indicates that the velocity will be low at that point, stagnation point. Further downstream, (i.e. window-roof transition) the pressure is decreased at the same time as the velocity rises, this correspond to to the *Bernoulli's Equation*.

$$p_1 + \frac{\rho V_1^2}{2} = p_2 + \frac{\rho V_2^2}{2} \tag{6}$$

$$p = static\,pressure$$

$$\frac{\rho V^2}{2} = dynamic\,pressure$$

The friction force is created due to shear stresses between the fluid and the surface of the body and will be the sum of all the shear forces in the fluid. The greatest contribution to the friction drag comes from the areas with attached flow.[14]

2.1.2 Drag and lift coefficient

The drag coefficient is a dimensionless quantity that describes a vehicles aerodynamic resistance and is a useful tool when comparing different vehicle shapes regardless of size and speed. The drag coefficient can be expressed as in Eq. (7). The drag coefficient can be divided into two components, a friction and a form component, as described in section 2.1.1.

$$C_d = \frac{F_D}{\frac{1}{2}\rho U^2 A} \tag{7}$$

where $\rho = air\ density$, $U = freestream\ velocity$, $F_D = drag\ force$ and $A = frontal\ area$

When air streams around a body there will be a pressure difference between the upper and lower part, if no separation occurs in the flow field the air on the upper surface will travel a longer path to reach the end of the vehicle. This difference in travel length will create a difference in the speed of the fluid, longer way to travel will give a higher speed, and lower pressure. On a vehicle the pressure will be lower on top of the vehicle and higher underneath it, this gives the lifting force (F_L). The lift coefficient is a dimensionless coefficient that describes the lift generate on the body and is expressed in Eq. (8).

$$C_l = \frac{F_L}{\frac{1}{2}\rho U^2 A} \tag{8}$$

2.1.3 Pressure coefficient

A useful parameter to compare incompressible flows is the *pressure coefficient* (C_p), see Eq. (9). The pressure coefficient (C_p) descibes how the pressure on a surface deviate from the freestream pressure. Every single point in the flow field or on the the surface has an unique C_p. To find the stagnation pressure on a surface C_p should be equal to one. If C_p instead is equal to zero this indicates a low pressure region where the risk for separation is high. In Eq. (9) the pressure coefficient is expressed in terms of pressure.

$$C_p = \frac{p - p_\infty}{\frac{1}{2}\rho V^2} = \frac{p - p_\infty}{dynamic\,pressure} \tag{9}$$

where p_∞ is the static pressure in the freestream and p is the pressure in the specific point.

2.1.4 Induced drag

Another important drag source is the induced drag(vortex drag), some times referred as trailing vortices, that is created from lift induced geometry such as a wing profile. Induced drag can even be generated from the pressure difference between the underbody and roof of the vehicle. Induced drag consists of drag created from an increased kinetic energy in form of increased vortex motion and additional viscous drag.[2]

2.2 Flow separation

As a body is moving through a fluid a boundary layer is formed near the surface where viscous forces occur. This boundary layer can either be of laminar nature or turbulent. To establish the type of boundary layer the *Reynolds number* can be calculated, see Eq. (10). The flow become turbulent for high Reynolds numbers.

$$Re = \frac{\rho U l}{\mu} \tag{10}$$

As the air travels along the surface of an immersed body (see Figure 3) the pressure gradient of the boundary layer drops. When the gradient of the velocity profile (boundary layer) reaches a value

of zero a separation of the flow will occur. As the flow separates the air becomes de-attached from the surface and will instead form eddy. This will result in increased drag or more specifically pressure drag which means that a delay in flow separation would have been more favorable in terms of total drag.

L. Prandtl showed that flow separation is caused by excessive momentum loss near the surface in a boundary layer moving against an increased pressure gradient ($\frac{dp}{dx} < 0$, *adverse pressure gradient*).

The equation of motion can be reduced to Prandtl's boundary layer equations for 2D incompressible flow which can be used to describe the velocity profile of the boundary layer and calculate the adverse pressure gradient.[14]

$$Continuity: \quad \frac{\partial u}{\partial x} + \frac{\partial v}{\partial y} = 0 \tag{11}$$

$$Momentum\ along\ wall: \quad \frac{\partial u}{\partial x} + v\frac{\partial u}{\partial y} \approx U\frac{dU}{dx} + \frac{1}{\rho}\frac{\partial \tau}{\partial y} \tag{12}$$

From these equation one can explain the flow separation by using the second derivative of the velocity [u] at the wall. By setting the $u = v = 0$ at the wall the Eq. (11) and (12) the adverse gradient can be calculated, see Eq. (13).

$$\left.\frac{\partial \tau}{\partial y}\right|_{wall} = \mu \left.\frac{\partial^2 u}{\partial y^2}\right|_{wall} = -\rho U\frac{dU}{dx} = \frac{dp}{dx} \tag{13}$$

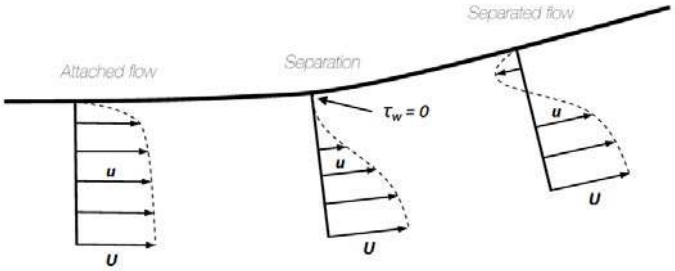

Figure 3: Boundary layer separation

The primary reason for boundary layer separation can be explained by Figure 3 that show how the velocity gradient along the surface changes direction. The point of separation (x_s) is defined when the pressure gradient of the slope is zero ($\tau_w = 0$).[8] Results from the simulations of each case will give the shear stress at the wall and will show at what location the flow will separate from the surface.

2.2.1 Separation On a Car and Wake Creation

The flow around a passenger car is asymmetric, the vehicle body consists of unevenness which will lead to separation of the flow. Two different types of separations can occur, *quasi-two dimensional* and *three-dimensional separation*. Quasi-two-dimensional occurs on edges perpendicular to the flow, such as the edge between the grill and hood. This kind of separation is characterized by high degree of turbulence. After separation the flow is able to reattach further downstream, if there is a surface

to reattach to. This type of separation occurs at the rear part of the vehicle and creates a big wake behind the car.

The other kind of separation is three-dimensional type and occurs around edges where the air flows with an angle, i.e. at the A- and C-pillars. Vortices are created and developed in the streamwise direction. This kind of trailing vortices are refereed as the induced drag, see Section 2.1.4 and Figure 4. The circulation depends on the shape of the edge where separation occur and the direction of the air that moves from the high pressure region to low pressure region.

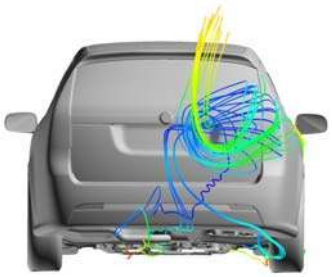

Figure 4: Induced drag on a passenger car

When a fluid flows along a body it will slow down nearest the body due to the friction from the surface. The decreased velocity result in an increased pressure which in turn means that the force to slow down the fluid exceeds the force to carry it forward. When this appears the fluid nearest the surface changes direction and separation occurs. A wake is created where the separation takes place, the wake has lower pressure then the surroundings. The lower pressure behind the body in combination with the higher pressure in front of it leads to an increase in drag resistance. By delaying the separation the size of the wake will decrease and also the drag.[14]

2.2.2 Underbody

A smooth underbody is necessary for a effective diffuser. A longer diffuser is more effective due to a more smooth increase in pressure and to avoid separation. (The same drag reduction can be achieved for a long diffuser as a short steep.)[5]

To achieve a effective diffuser as possible the flow should be attached along the whole diffuser. Attached flow can be achieved by having a long flat underbody so the flow separates early under the vehicle and then reattach before the diffuser starts. A to high diffuser angle can however make the flow to separate at the edge.

A smooth underbody will not only affect the effect of the diffuser. According to *R.H. Barnard* the underbody contributes to the total drag with around 20 percent, due to the roughness of the underbody.[2]

2.2.3 Rear-end

85 percent of the total drag is generated from the form drag also called pressure drag.[10] By lower the pressure difference between the front and rear, i.e. increase the base pressure, the drag coefficient should rapidly decrease. A higher base pressure can be achieved by decrease the area of the rear end, this means that the vehicle has to be extended and have a more teardroped shape. Due to

environmental circumstances a vehicles length is restricted, so too increase the base pressure other methods have to be implemented, for example introducing a *diffuser*. The rear-end of the vehicle plays an important role since the effect of the diffuser is depending on the shape of the rear-end, as well as the separation is dependent on the shape.[6]

There are three kinds of common rear-ends for passenger cars, *notchback* (sedan), *hatchback* and *squareback* (wagon). The design of the rear-end has a big influence on the behavior and shape of the wake. When designing the rear-end the aim is to make the base pressure as high as possible and get a low pressure difference between the stagnation pressure in the front and the base-pressure in the rear. A squareback has a relative high rake angle (ϕ), see Figure 5a. This high rake angle makes the flow separate early and not stay attached over the rear windscreen. If the flow would remain attached it could create a strong downwash of the flow field which cause a high degree of turbulence in the wake, this would increase the drag. This type of behavior is common on hatchbacks with a rake angle near 30°and trailing vortices would be created to some extend and the induced drag will be increased. A high rake angle decreases the downwash and the induced drag but will on the other hand have an negative impact on the pressure drag.[2]

One of the most efficient ways to reduce the drag resistance is to balance the wake, in order to do so the design of the underbody should approximately be the same as the upper part of the rear-end. For a squareback, where the separated region originates directly from the roof edge, the underbody/diffuser should be quite flat in order to match the roof.[5]

On the rear of the notchback it's possible to recognize both quasi-two-dimensional and three-dimensional separation. On a notchback there are three parameters on the rear that affects the drag: the height, z, and length, x, of the notch and the inclination, γ, of the rear window, see Figure 5b. Generally a higher boot will generate a lower drag, as well as a greater inclination of the rear window.[5]

In the region between the boot and the window a so called dead water region is created due to separated flow on the rear window. In the dead water region the flow is recirculating, further downstream the flow is re-attached. In some cases the trailing vortices created around the C-pillars are affecting the flow over the trunk which results in no re-attachment and a strong downwash. If the flow is re-attached it will cause a pressure rise on the boot and the drag will then be reduced. In the case with the *SAAB 9-3 Sedan* the inclination, γ, is not that steep and the flow will reattach on the notch.

The wake on the *SAAB 9-3 Sedan* will however be directed downwards against the ground, by introducing a diffuser at the underbody the balance of the wake will be improved and more symmetric.

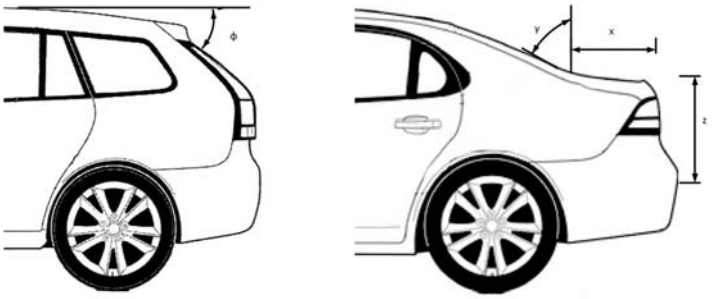

(a) Wagon (b) Sedan

Figure 5: The rear-ends of the wagon and sedan

2.3 Diffuser

Diffusers have been used on racing cars in decades, however in the last few years when fuel economy has become one of the most important issues for the automotive companies and diffusers have become an option for drag reduction even for passenger cars. In this section the function of a diffuser will be explained according to the theory presented earlier.

2.3.1 Diffuser Theory

One of the main functions of a diffuser is to create downforce, this is achieved by improving the transition between the high velocity airflow underneath the body and the slower airflow around the vehicle. The underbody is designed as a *convergent-divergent "venturi" channel* with the road which generates a low pressure region that "sucks" the car to the ground. A diffuser will generate more downforce then a wing[7], and will also produce less trailing vortex drag. As the air flows underneath the body, the flow will have a negative pressure peak where the diffuser starts, see Figure 6. In front of the diffuser the flow will accelerate and decrease the pressure which generates downforce according to Bernoulli´s law.

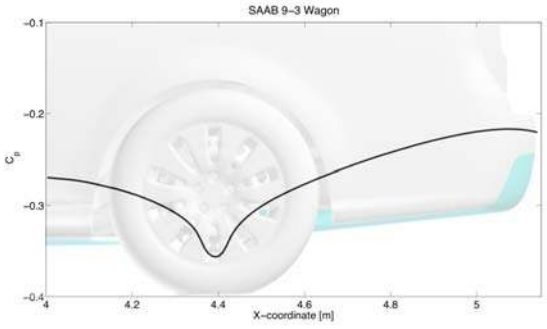

Figure 6: Diffusers impact on the downforce

In the diffuser the cross-section area increases, a bigger area will decrease the velocity of the fluid and increase the static pressure. A high static pressure recovery in the diffuser will lead to a higher base pressure. According to *Cooper* there are three non-dimensional parameters that affects the properties of a diffuser, the *area ratio*, the *non-dimensional diffuser length* and the *diffuser angle*. In Figure 7 a schematic picture of a diffuser is shown with the most important parameters displayed.

- Area ratio: $\frac{h_2}{h_1}$
- Non-dimensional diffuser length: N
- Diffuser angle: θ

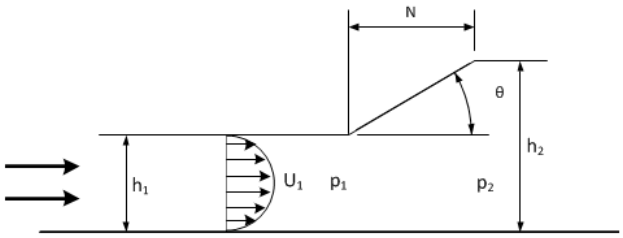

Figure 7: Schematic figure of a diffuser

The shape of the velocity profile in Figure 7 depends on the underbody's proximity to the ground as well as the roughness and the length of the entry section (before the diffuser). With a smooth underbody the flow will remain attached which is favorable. The velocity profile will have a different shape if the simulation is performed with a moving ground system, since there will be no boundary layer growth on the ground.

According to *G. Sovran & Cooper[7]* the mechanisms to generate downforce and reduce drag can be divided into three sections:

- **Upsweep** - The rear end of the underbody will camber the flow and due to Bernoullies's equation the base pressure will increase.

Vehicles with higher ground clearance the upsweep of the underbody is a good tool to reduce the drag when matched correctly with the upper rear-end geometry of the car. The variable parameter is the *diffuser angle* which is a key variable in this study.

- **Ground interaction** - A symmetrical body that is exposed to wind, or traveling through air has no lift force. By placing this body in proximity to the ground it will result in a asymmetrical flow which will accelerate underneath the body. The increased air velocity will decrease the static pressure and generate a downforce or negative lift force. The downforce is increasing with proximity to the ground.

The ground interaction affects the drag in both an inviscid and a viscous way. The inviscid effect will increase the drag by moving the stagnation point in front. The viscous effect becomes significant on small ride heights when the boundary layer will connect to the ground, i.e. no greater impact on passenger cars.

- **Diffuser pumping** - The cross-section area in a diffuser increases downstreams which results in a reduction of the air velocity. If no separation of the flow occurs, the greater the cross-section area becomes, the greater the static pressure becomes. The pressure rise is a function of the ratios of the inlet and outlet area. These areas are depending on the diffuser angle and the ride height of the vehicle.

Diffuser pumping will always increase the downforce, how much is depending on the ride height. Diffuser pumping will also increase the drag. According to G. Sovran's the projection of the inclined diffuser are related as in Eq. (14).

$$C_D^{diffuser} = tan\theta \left(-C_L^{diffuser}\right) \tag{14}$$

I.e. an increased downforce will increase the drag, but only for the diffuser pumping contribution.

To compare different diffuser designs Sovran referred to the static pressure recovery coefficient for a diffuser, Eq. (15). A good drag reduction diffuser would then have a high C_{pd}.

$$C_{pd} = \frac{p_2 - p_1}{\frac{1}{2}\rho U_1^2} \tag{15}$$

There has to be a trade-off between downforce and drag, since the upsweep reduce the drag while the diffuser-pumping increase it depending on the ride height. On lower ride heights the total drag will increase, as for high performance cars. To minimize the drag the ride height should be set so the behavior of the car will not be affected, i.e. not to low and not to high.

2.4 Computation Fluid Dynamics (CFD)

CFD is a numerical method to compute and analyze the dynamics of a fluid. The approach for a CFD simulation is to divide the physical domain into small finite volume elements where the governing equations are solved numerical. Almost all flows are turbulent, to spare computer capacity so called turbulence models can be used to simulate the turbulence. In the following sections the governing equations are presented as well as turbulence models.

2.4.1 General CFD

In fluid dynamics there are three governing equations, also described in Section 2.1, that describes the behavior of the flow, these are the *continuity*, *momentum* and the *energy* equations. They are derived from basic physics laws such as the conservation of energy, mass and momentum. These equations becomes rather complicated and can't be solved analytic so numerical simulations are required. In a

CFD simulation the differential equations are discretizised into large systems of algebraic equations in order to numerical solve them. Since vehicles travels at relatively low speed, Ma<0.3, and constant temperature the flow can be assumed incompressible and isothermal[10], the energy equation can then be neglected.

Navier-Stokes equation Navier-Stokes equations are derived from Newtons second law and can be seen as a force equilibrium for an infinitesimal small volume element. In order to convert the stresses to velocity components the Navier-Stokes equations are usually expressed for an incompressible Newtonian fluid with constant viscosity. An incompressible fluid is a fluid where the divergence of the velocity is zero, and a Newtonian fluid is a fluid which stress versus strain rate curve is linear. The Navier-Stokes equations can then be expressed as in Eq. (16), three partial non-linear differential equations, one for each velocity vector.[14]

$$\begin{aligned} \rho g_x - \frac{dp}{dx} + \mu\left(\frac{d^2u}{dx^2} + \frac{d^2u}{dy^2} + \frac{d^2u}{dz^2}\right) &= \rho\frac{du}{dt} \\ \rho g_y - \frac{dp}{dy} + \mu\left(\frac{d^2v}{dx^2} + \frac{d^2v}{dy^2} + \frac{d^2v}{dz^2}\right) &= \rho\frac{dv}{dt} \\ \rho g_z - \frac{dp}{dz} + \mu\left(\frac{d^2w}{dx^2} + \frac{d^2w}{dy^2} + \frac{d^2w}{dz^2}\right) &= \rho\frac{dw}{dt} \end{aligned} \tag{16}$$

Continuity equation The continuity equation is based on the principle that the mass is indestructible, and can be written as Eq. (17).

$$\frac{\partial\rho}{\partial t} + \frac{\partial(\rho u)}{\partial x} + \frac{\partial(\rho v)}{\partial y} + \frac{\partial(\rho w)}{\partial z} = 0 \tag{17}$$

Since the flow is assumed incompressible the continuity equation will be as in Eq. (18).

$$\frac{\partial u}{\partial x} + \frac{\partial v}{\partial y} + \frac{\partial w}{\partial z} = 0 \tag{18}$$

Together with the Navier-Stokes equation the Continuity equation gives four unknowns, u, v, w & p, which will be solved with differential equations.

2.4.2 RANS

The non-linear partial differential equations are not analytically solvable. In order to solve these equation and analyze the flow the simplest approach is the Reynolds decomposition, also called *Reynolds Average Navier Stokes* (RANS).[4] In the RANS approach the instantaneous velocity and pressure is split into two parts, an average part and a fluctuating part, Eq. (19) and Eq. (20).

$$\overline{u} = \frac{1}{T}\int_0^T u\,dt \tag{19}$$

$$\begin{aligned} p &= \bar{p} + p' \\ u &= \bar{u} + u' \\ v &= \bar{v} + v' \\ w &= \bar{w} + w' \end{aligned} \tag{20}$$

Inserting *Reynolds decomposition* into Navier-Stokes equation (x-direction) and in the continuity equation will results in new fluctuating terms.

$$\frac{\partial \bar{u}}{\partial x} + \frac{\partial \bar{v}}{\partial y} + \frac{\partial \bar{w}}{\partial z} = 0 \tag{21}$$

$$\rho g_x - \frac{\partial \bar{p}}{\partial x} + \frac{\partial}{\partial x}\left(\mu \frac{\partial \bar{u}}{\partial x} - \rho\overline{u'^2}\right) + \frac{\partial}{\partial y}\left(\mu \frac{\partial \bar{u}}{\partial y} - \rho\overline{u'v'}\right) + \frac{\partial}{\partial z}\left(\mu \frac{\partial \bar{u}}{\partial z} - \rho\overline{u'w'}\right) = \rho \frac{d\bar{u}}{dt} \tag{22}$$

Eq. (22) now consists of new unknown terms like $\rho\overline{u'v'}$, also called for *Reynolds stresses*. Since the number of unknowns are greater then the number of equations a so called *closure problem* is generated, the extra stress terms has to be modeled to get a closed equation system. This is done by using turbulence models.[14]

2.4.3 Turbulence flow and turbulence modeling

The largest difficulty with CFD simulations is to calculate the turbulent flow. A turbulent flow is irregular and varies randomly in time and space. With existing computer capacity it's impossible to solve Eq. (16) and (18) exact. By using so called turbulence models the flow field can be calculated with less computer capacity. Such a model will modify the equations and only consider the average effects of the turbulence. The flow will then be divided into an average term and a fluctuation term, this can be done using *Reynolds Average Navier Stokes* (RANS). A turbulence model can never give an exact solution, but a better choice will give an more accurate solution. The choice of model is a matter of computer capacity and required level of accuracy.[3]

$k-\epsilon$-model The $k-\epsilon$-model is the most commonly used turbulence model in the industry, this due to the robustness of the model which gives safe convergence. A good overview of the flow field is achieved with the model, but in areas with high velocity and pressure gradients the accuracy is not that high. The $k-\epsilon$-model is an *Eddy Viscosity model,* which means that the turbulence is modeled by adding the turbulence viscosity, μ_t. This model is a semi-empirical method based on how the kinetic energy, k, is transported and its dissipation rate, ϵ. The transport equation for k is derived exact while the transport equation for ϵ is derived from physical reasoning.[1] The biggest eddies gets their *kinetic energy*, $k = \left(\triangle u^2 + \triangle v^2 + \triangle w^2\right)^{1/2}$, from the main flow. The energy is transmitted into smaller eddies and ends up as internal energy. Since the $k-\epsilon$-model is a RANS-model and is using time average terms the model will miss differences in the gradients during very short time steps.

In order to achieve a more accurate solution of the flow a new model has been developed called the *$k-\epsilon$-realizable*.[1] This new model has a new formulation for the turbulent viscosity, transport equation and for the dissipation rate. In the derivation of the *standard $k-\epsilon$-model* the flow is assumed to be fully turbulent, which makes the model only valid for these circumstances. In the *realizable $k-\epsilon$-model* the normal and molecular stresses are taken into account to some extend. The relationship between the kinetic energy, the dissipation rate and the turbulent viscosity is defined in Eq. (23).[13]

$$\mu_t = C\mu\rho\frac{k^2}{\epsilon} \tag{23}$$

As mentioned an extra term, $\rho\overline{u'v'}$, is included in the Navier-Stokes equation. In the $k-\epsilon$-model the extra stress term is modeled with a Boussinesq assumption, see Eq. (24).

$$-\rho\overline{u_i'u_j'} = \mu_t\left(\frac{\partial u_i}{\partial x_j}+\frac{\partial u_j}{\partial x_i}\right)-\frac{2}{3}\left(\rho k+\mu_t\frac{\partial u_i}{\partial x_i}\right)\delta_{ij} \tag{24}$$

2.4.4 Boundary layers and wall functions

When a fluid flows along a body a boundary layer is created near the surface. Near the surface the velocity of the flow is zero, the velocity grows and reaches the freestream velocity. The thickness of the boundary layer is defined as the distance from the body to where the velocity reaches 99% of the freestream velocity. The boundary layer can be divided into three parts, one laminar, one turbulent and a mixture of them both, see Figure 8. The boundary layer starts as laminar when the body is exposed to the fluid, as the fluid develops along the body it becomes more and more turbulent. A laminar boundary is to prefer since the skin friction is lower then for a turbulent layer in certain applications.

The near wall flow is usually divided into three regions, the *viscous sublayer*, the *buffer layer* and the fully turbulent *log-law region*. Figure 8 shows the near wall region, here plotted with semi-log coordinates. On the y-axis there is the non-dimensional wall distance, y^+, which is defined as in Eq. (25).

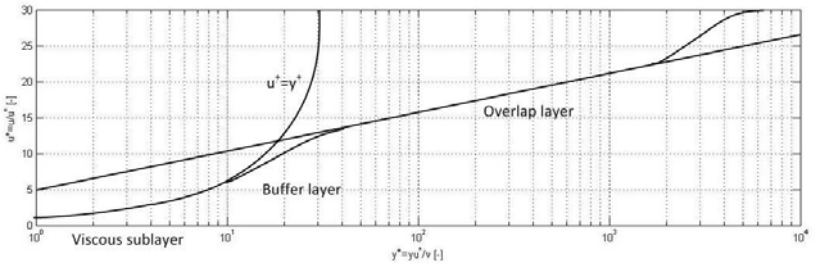

Figure 8: Velocity profile in the near wall region for a turbulent boundary layer

$$y^+ = \frac{yu*}{\nu} \tag{25}$$

$$u* = 0.05U \tag{26}$$

where $u*$ is the friction velocity (Equation 26) , ν is the kinematic viscosity and y is the height of the first cell.[14]

In order to solve the velocity profile in the boundary layer wall functions have been used. In normal case (without wall functions) the thickness of the first cell must have a $y^+ = 1$, but by using wall functions y^+ can vary between 30 and 300. In Fluent there are two kinds of wall functions, *standard wall functions* and *non-equilibrium wall functions*. Wall functions assumes that the flow near the wall behaves fully turbulent and use the algorithm to resolve the gradients in the boundary layer. In the non-equilibrium wall functions the sensitivity for the pressure-gradients are higher then for the standard wall functions. The non-equilibrium wall function predicts the flow better in domains where

the geometry is complex and separation with reattachments frequently appear. This is due to the capability to account the pressure-gradient effects.[1]

2.4.5 Fluent Set-up Solver

In the Fluent software there are two kinds of solvers, *pressure-based* and *density-based*. The pressure-based solver has been used in this study since the solver is suited for incompressible flows and low velocities.[1] To resolve the flow the domain has been divided into discrete control volumes. In each control volume the governing equations will be integrated to a algebraic equation system which will be linearized and solved for each iteration. The governing equations can be solved either separate (SIMPLE or SIMPLEC) or coupled (COUPLED) depending on which algorithm that is used. SIMPLE is to prefer when the simulation is steady state and the computer capacity is limited. COUPLED is a more robust and safer method which gives better convergence. When running transient simulations there are other requirements of the solver, in such simulations SIMPLEC or PISO are preferred. Using SIMPLEC on a steady state simulation can lead to instability.

2.4.6 Discretization and iteration

To be able to analyze the flow field the governing equations has to be written as integrals and the total domain has to be divided into small cells, see Section 2.4. Each cell consists of six faces and the flow in each cell is depending on its neighboring cells. There are different calculating schemes for calculating the governing equations, in this investigation the first and second order upwind scheme have been used. In a first order upwind solution scheme the governing equations are solved by interpolating the solution from one neighbor cell in each direction. In a second order upwind scheme the equations are solved by using two neighbor cells in each direction. The second order upwind scheme gives a more accurate result but needs more computer capacity.[4]

2.4.7 Mesh/Domain

The computational domain is designed to lead to a free flow with neglectable blockage, which essentially means a box that consists of a inlet, a outlet, two sides, a roof and a ground surface. This domain was included in the *ANSA*-model that was provided from *SAAB Automobile*. The size of the domain is approximately three vehicle lengths upstream and eight vehicle lengths downstream from the model, the cross section area is around eight times the vehicle height high and approximately ten times the vehicle widths wide. The total dimensions are presented in Table 1 and the domain is illustrated in Figure 9.

Table 1: Dimension of the domain

Height	12 [m]
Length	61 [m]
Width	20 [m]

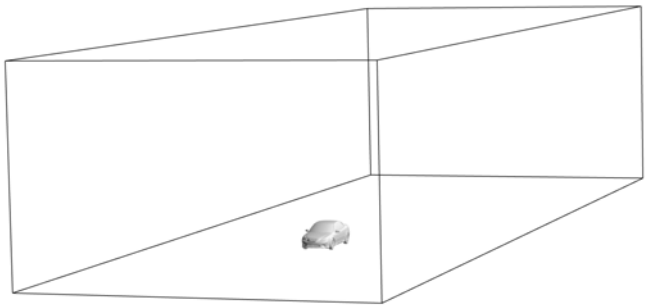

Figure 9: The domain

The surface mesh was created on the geometry of the vehicle as well as on the surface of the domain. Between the surface of the vehicle and the domain the computational grid was generated. To capture certain areas of interest (where separation might occur and where the degree of turbulence is high) the cells have to be small enough to solve all irregularities and achieve a robust solution. The grid has been refined around the car, at the rear and specially underneath the vehicle since this study is focusing on the underbodys influence on the flow field. These refinement zones can be seen in Figure 10. In the refinement zones the cell size is between *~10-20* mm.

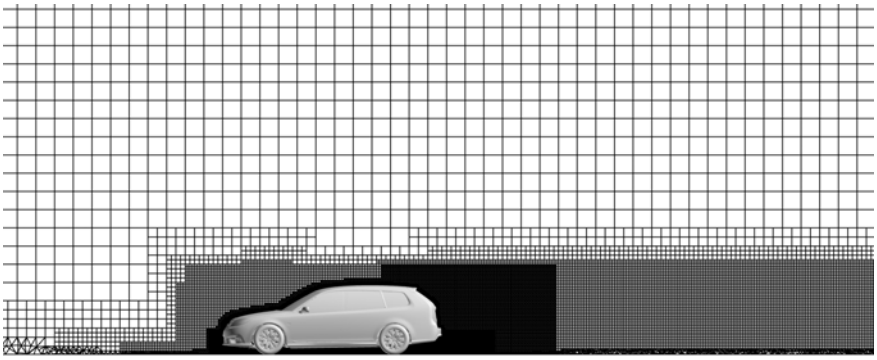

Figure 10: Refinement zones around the vehicle

In previous sections it has been mentioned how the air act when flowing past a surface and create a boundary layer. To capture this flow phenomena a refinement region around the the exposed surface must be created, this refinement area is called a *prism layer*. It's important to define the orientation of the surfaces in order to make the prism layer to grow in the direction of the normal vectors. On the vehicle body prismatic layer has been used to reach the right y^+value, *~200-300*, see Figure 11. The prismatic layer is needed to predict the flow more accurate since the highest gradients are located near the wall.

The height of the cells in the prism layers is estimated using Eq. (25) and (26).[14] In this study the number of layers has been set to five with an geometric growth rate of 1.2 and a first aspect ratio

of 5. An aspect ratio of 5 means that the first prism layer has an height of 1/5 of the surface mesh length.

The computational grid is of the type *hexcore* (quadratic cells) which is used to spare the number of total cells, in overlap regions between the prism layer and the hexcore tetrahedral cells have been used, Figure 11.

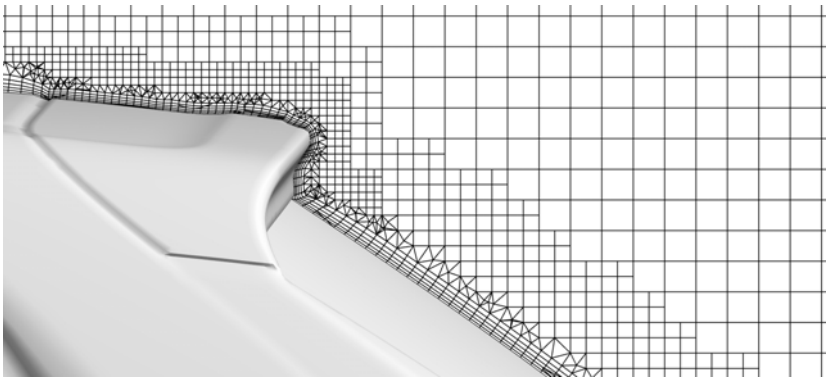

Figure 11: Prism and buffer layers on the vehicle

2.4.8 MRF-zones (Multiple Reference Frame)

In regions where the flow have different properties compared to the freestream flow multiple zones are preferred, e.g. the rotating wheels Figure 12. Inside the rims the fluid has an rotational speed, not a translational. By dividing the domain into multiple reference frame (MRF) zones the flow will be better predicted. The method does not account for the relative motion of the geometry, which means that the mesh is fixed. In applications where large velocity gradients occurs a sliding mesh approach are to prefer but in the case with rotating wheels the MRF-method gives sufficient accurate result.[1]

Figure 12: MRF-zone of the wheel

3 Case description

The governing motivation for this study is to investigate the possibility to reduce the overall drag by implementing a diffuser. In order to prove this theory a number of cases with different geometric setups must be done, but some limitations must be considered otherwise an infinite number of cases have to be simulated. In Figure 13 the *SAAB 9-3 Sport sedan* and *SAAB 9-3 Sports wagon* CAD-model is shown which where provided by *SAAB Automobile AB*.

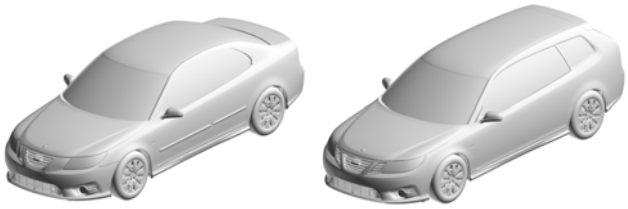

(a) Sedan (b) Wagon

Figure 13: SAAB 9-3 CAD-models

3.1 Reference

To measure any improvement by implementing additions as a diffuser there must be reference values generated by simulating the *SAAB 9-3 Sport sedan* and *SAAB 9-3 Sport wagon* without any geometric modifications. SAAB Automobile provided CAD models of these models which only subjected to minor alterations. In this investigation there is a focus on the underbody shape and geometry, in Figure 14 the unmodified underbody of the two CAD-models are shown. Figure 14 shown the detail level on the undercarriage which in this case requires a high resolution of the numerical mesh in order to resolve the air flow in a correct manner.

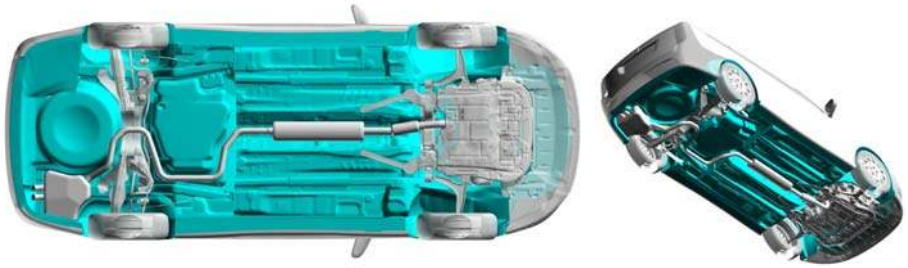

Figure 14: The underbody for the reference model

It can also be noted that the unmodified underbody (Figure 14) also shows the possibility to cover certain areas in order to reduce the roughness of the underbody. To simulate the air flow though the engine bay the radiator is constructed by implementing a perforated surface and measuring the mass-flow. From psychical test data on the mass-flow was provided by *SAAB Automobile* which was used as a guideline for the air flow through the radiator.

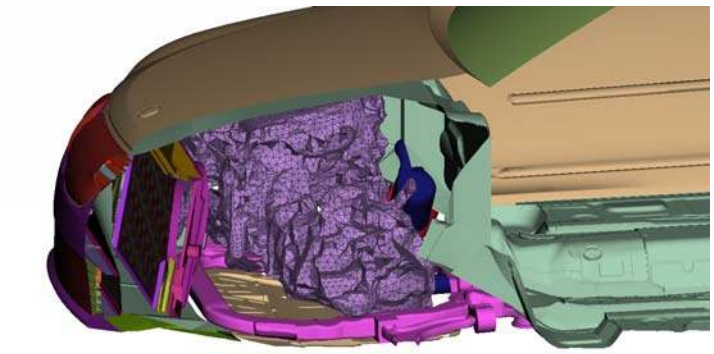

Figure 15: ANSA-model of the engine bay

Figure 15 shows the geometry of the engine which is mesh-wrapped in order to avoid small cavities which are hard to generate a sufficient numerical mesh.

3.2 Diffuser sweep

By placing the throat of the diffuser at a fix position at the center of the rear wheels hubs the angle of the diffuser can be the only parameter that significantly alters between each simulation. In this approach an optimal angle in terms of low drag can be achieved. From these initial results other cases with other modifications can be simulated with a low drag diffuser angle as a starting point. The different angles that were simulated was altered between three and 14 degrees, see Table 3. In Figure 16 the definition of the diffuser angle and the start of the diffuser throat are shown.

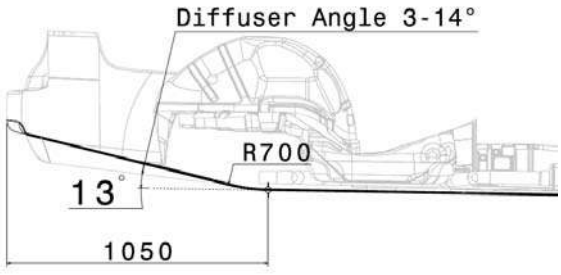

Figure 16: Side section view of the diffuser

It should be noted that the entire vehicle has an angle against the ground of 1° (higher ground clearance in the rear) but the diffuser angle is defined from the underbody.

To increase the possibility for attached flow in the region of the diffuser a covering of the entire underbody is done, see Figure 17. The covering of the underbody were done to the extend where the exhaust system och area for the rear suspension is kept open. This is done in order to have some heat

transfer from the exhaust system and the open areas around the rear suspension is there due to the movement of the suspension.

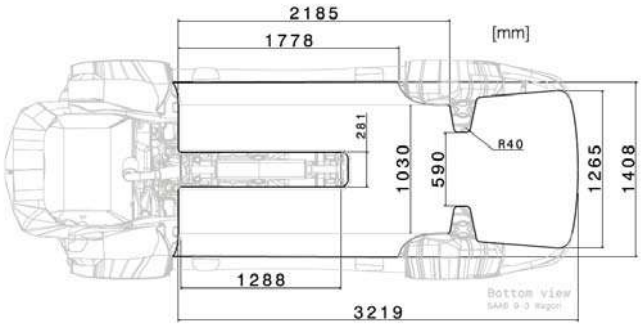

Figure 17: Diffuser and covering of undercarriage, bottom view

In Figure 18 illustrates the necessary modifications to the exhaust silencer and rear trunk in order to implement this type of diffuser.

Figure 18: Intersection between diffuser and unmodified underbody

In order to calculate the drag coefficient the *frontal area* (A_f) must be provided which can be found in Table 2. The table shows an increase in the frontal area due to the implementation of the diffuser and also the length and wheelbase.

Table 2: Frontal area (A_f)

Model	9-3 Sedan	9-3 Sedan + diffuser	9-3 Wagon	9-3 Wagon + diffuser
Projected frontal area [m^2]	2.1897	2.1992	2.2451	2.2546
Length [m]	4.63	4.63	4.63	4.63
Wheel base [m]	2.675	2.675	2.675	2.675

3.2.1 Diffuser design

Different solutions to the design of the diffuser has been simulated which mainly differ in the rear region of the diffuser. The reason for the different concepts is the change in effective length and aesthetics. Figure 19 shows the difference in design on the station wagon with a diffuser angle of *5°*.

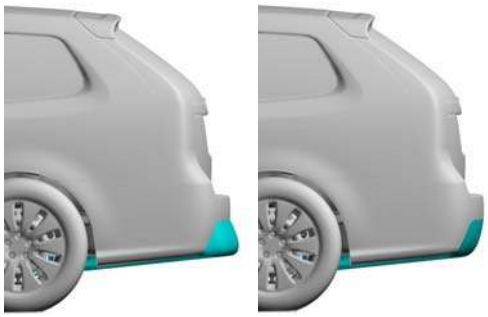

(a) Design #1, 5° diffuser (b) Design #2, 5° diffuser

Figure 19: Comparison different diffuser designs for wagon

3.3 Vortex generators

Section 2.2 described the benefits of attached flow and device to delay separation of the flow can be a so called *vortex generator*. The vortex generator disturbs the flow and can make the air flow reattach by generating a turbulent boundary layer. In order to implement a vortex generator the point of separation is needed to place the vortex generators. In Figure 20 the *SAAB 9-3 Sports wagon* with a diffuser that has an 8 degrees angel is shown and which illustrates the wall shear stresses in order to determine the point of separation on the diffuser. The figure shows that the main separation occurs at the sides (blue region) of the diffuser due to the opening for the rear suspension. By implementing vortex generators some of that flow can be reattached.

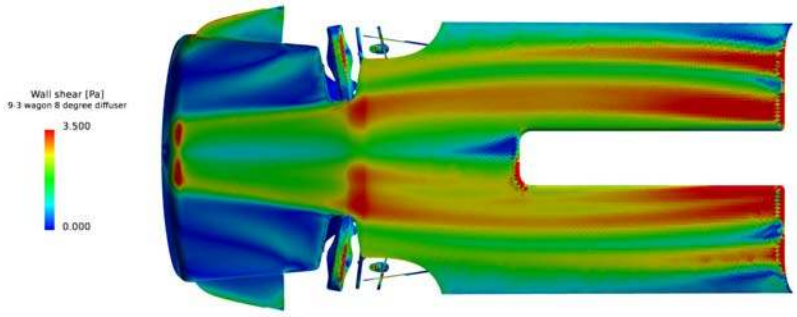

Figure 20: Wall shear stresses for the original diffuser

The general shape and size is based on assumptions when the efficiency is at its best. The results can be misleading without doing a deep analysis of the effects of implementing vortex generators. With this said the implementation of the VGs is a small side step from the scope of this project. In Figure 21 the geometry of the vortex generators is shown, which has a half delta wing shape. The wing profile used for constructing this vortex generator is an *NACA23012* wing profile which is commonly used in the aircraft industry.

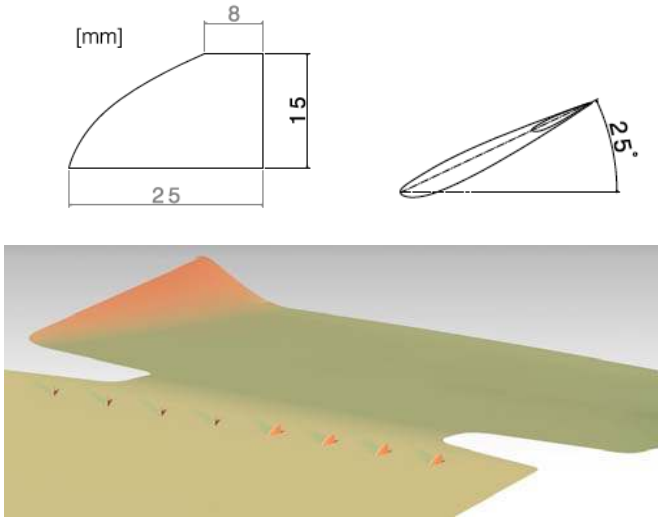

Figure 21: Geometry of vortex generators

The vortex generators where placed 25 degrees to the freestream air direction which has showed positive results in other applications.[9] Figure 21 shows the height of the vortex generator which is an approximation of how large the boundary layer could be at that location.

3.4 Guiding vanes

The use of "guiding vanes" or "turning vanes" in the diffuser has the intend function to guide the air flow trough the sloped area in order to expand the air in the desired way. The increased friction drag is redundant but an induced vortex can be formed due to the introduction of the guiding vanes which both can separate and maintain attached airflow. These vanes can also be useful in areas where the underbody airflow will experience lateral gusts, typical near the rear axle line. The lower pressure in the throat of the diffuser suck in air from the sides and vertical mounded vanes will help to let the longitudinal flow to stay attached. The overall geometry of these vanes is high depended on the specific vehicle and application, but with these previously mentioned guiding tips a suitable geometry can be obtained.[11][12]

In the step of constructing and implementing the guiding vanes a trail and error approach is used. The number of vanes used where 2, 3 and 4 in Figure 22 the different cases are shown. Another important demand was that the vertical measure did not exceed the original ride eight in the rear part of the vehicle.

The introduction of these vertical vanes also made it possible to expand the oncoming airflow in a lateral way and hopefully increase the efficiency of the diffuser and increase the pressure recovery. A cases with no lateral angle was also simulated in Figure 22 the difference in design can be seen.

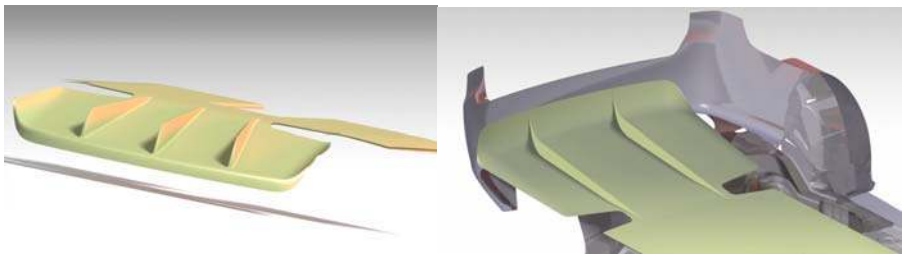

(a) 12° diffuser with 3 lateral angeled GVs (b) 8° diffuser with 2 GVs

Figure 22: CAD-models on guiding vanes

3.5 Flat rim

The flow that originates from the rear wheel has a major impact on the air flow in the diffuser and by restricting this flow some interesting results can be obtained. This case then simply be performed by covering the rims and restricting the flow through the MRF-zone, Figure 23. It should be pointed out that this has a major influence on the cooling of the brakes but this is beyond the scope of this study.

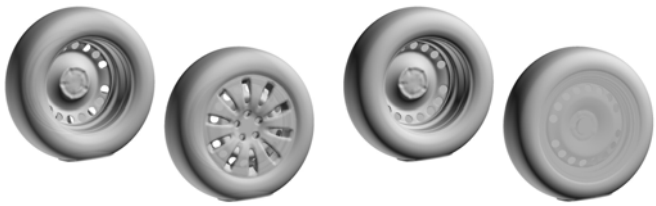

(a) Original rims (b) Flat rims

Figure 23: Comparison between original and flat rims

3.6 No underbody covering

By introducing cover-plates on the underbody the ground effects should be affected significantly due to the reduction in ride height and overall smoothing of the underbody surface. So to measure the diffusers absolute effect on the pressure wake a case was prepared where there is no coverplates on the underbody. The angle of this diffuser is based on the simulated results from the previous cases with underbody covering. In Figure 24 a picture of the case is displayed to show the attempt to eliminate sharp edges and overall design.

Figure 24: Configuration with only diffuser and underbody panel

3.7 Covering of the rear suspension

Since the rear suspension is affecting the flow onto the diffuser it would be interesting to simulate a case with the suspension covered. In Figure 20 it could be noted that the flow is separated at the rear suspension which causes a small effective area on the diffuser to reduce drag. In order to see how a completely flat underbody should affect the total drag resistance the link arms of the rear subframe was removed and the holes where covered, see Figure 25.

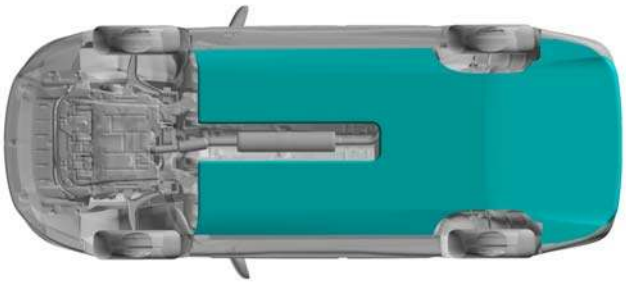

Figure 25: Configuration with flat underbody, covered rear suspension

3.8 Test matrix

In this section a table of all the cases that where simulated are presented to get an overview of the extend of this investigation, see Table 3. Abbreviation of each case has been done in Table 3 in order to make the cases more manageable.

Table 3: CFD Test matrix

Diffuser angle [deg]	14°	12°	10°	8°	5°	3°
SAAB 9-3 SEDAN MODEL	-	-	-	-	-	-
Reference ($S1, \surd$)	-	-	-	-	-	-
Diffuser with underbody covering (D&UC)	$S2, \surd$	$S3, \surd$	$S4, \surd$	$S5, \surd$	$S6, \surd$	-
D&UC and 2 guiding vanes	-	-	-	$S7, \surd$	-	-
D&UC and 3 guiding vanes	-	$S8, \surd$	-	-	-	-
D&UC and 4 guiding vanes	-	-	-	$S9, \surd$	-	-
D&UC and vortex generators	-	$S10, \surd$	-	-	-	-
D&UC and rear suspension covering	-	-	-	$S11, \surd$	-	-
Diffuser with NO underbody covering	-	-	-	$S12, \surd$	-	-
D&UC and covering of rear wheel rims	-	-	-	$S13, \surd$	-	-
D&UC and covering of all wheel rims	-	-	-	$S14, \surd$	-	-
SAAB 9-3 WAGON MODEL	-	-	-	-	-	-
Reference ($W1, \surd$)	-	-	-	-	-	-
D&UC design#1	$W2, \surd$	$W3, \surd$	$W4, \surd$	$W5\surd$	$W6, \surd$	$W7, \surd$
D&UC design#2	-	-	-	$W8, \surd$	$W9, \surd$	$W10, \surd$
D&UC and 2 guiding vanes	-	-	-	$W11, \surd$	$W12, \surd$	-
D&UC and 3 guiding vanes	-	$W13, \surd$	-	-	-	-
D&UC and vortex generators	-	-	-	$W14, \surd$	-	-
Diffuser with NO underbody covering	-	-	-	-	$W15, \surd$	-
D&UC and covering of rear wheel rims	-	-	-	-	$W16, \surd$	-
D&UC and covering of all wheel rims	-	-	-	-	$W17, \surd$	-

3.9 Boundary conditions

The solver used for these simulation is *Fluent 13.0* and in Appendix A a script file is presented which shows all the different settings. In this section a short description of the boundary conditions are presented in order to give an overview of the driving conditions during the simulation, see Table 4. A well established wind speed or driving speed within the automotive industry when simulating a road vehicle is *140 km/h* (*38.89 m/s*) and this speed is also used in this investigation. At this velocity the density can be assumed to be constant and the governing equations are then pressure based and the flow is incompressible. Another well documented practice within CFD-simulations is the use of the realizable $k - \varepsilon$ turbulence model together with non-equilibrium wall-functions when solving the RANS-equations in Fluent, which will also be used during this project.[1]

Table 4: Boundary conditions

Surface/Part	Movement	Type	Condition
Tunnel-roof	stationary	symmetry	-
Tunnel-sides	stationary	symmetry	-
Tunnel-floor	transitional x-velocity	wall	38.89 [m/s]
Tunnel-inlet	stationary	velocity-inlet	0° yaw & 38.89 [m/s] turb. length scale: 1 [cm] turb. intensity: 0.1%
Tunnel-outlet	stationary	pressure-outlet	Guage pressure: 0.0 [Pa] turb. length scale: 1 [cm] turb. intensity: 0.1%
Vehicle	stationary	wall/interior/fan	no-slip
Wheels	rotational velocity (y-axis)	wall	no-slip 123.186 [RPM]
MRF-zones (Moving reference Frame)	rotational velocity (y-axis)	wall/fan	123.186 [RPM]

To model the flow resistance through the radiator a perforated surface is used to restrict the air flow, this method is currently used by *SAAB Automobile* and a deviation from this method did not seem necessary. An alternative method could be done by alternatively using a porous medium and modeling the pressure drop and inertia and viscous resistance in the radiator more accurately.

Table 5: Rotational coordinates

Y-axis coordinates [m]	x	y	z
Front wheel	1.726906	0	0.3157014
Rear wheel	4.402906	0	0.3157015
Vehicle (pitch moment)	3.058	0	0.384

Table 5 shows the rotational center for the boundary conditions regarding the wheels and MRF-zones and as well the rotational center of the entire vehicle which is used to determine the alterations in pitch moment between each simulated case.

3.10 Simulation in Fluent

By running the calculations for *3000* iterations shown to be adequate in order to achieve low residuals values. The first *500* iterations is done by calculating the RANS equations in first order and the next 2500 iterations is done by solving the second order of the numerical mesh.

The final *drag coefficient* (C_d) and *lift coefficient* (C_l) for each simulation is determined by calculating the mean value of the last *200* iterations.

4 Results

To be able to analyze the different configurations a detailed analysis of the unmodified reference models are done in order to get an overview of the flow behavior and establish a starting point for improvements.

4.1 Reference *SAAB 9-3 Sport sedan* and *SAAB 9-3 Sports wagon*

When comparing designs and shapes of different vehicles the dimensionless drag coefficient, C_d, is used. For passanger cars a normal value is about 0.3. In this study the reference sedan had a C_d of 0.2875 and the reference had a C_d value of 0.3033.

4.1.1 Energy losses

Figure 26 shows the two models with so called *iso-surfaces* for total pressure equal to zero, this irregular surface shows the wake formed behind the cars. A wake is an area of low pressure and a region of high turbulence that indicates a loss in energy. As can been seen in the figure wakes are also formed at the wheels, the mirrors and on the underbody. Here the iso-surfaces are colored with turbulence intensity to detect the most turbulence areas. Turbulence intensity is the ratio between the standard deviation of the velocity fluctuations and the mean velocity, see Eq. (27).

$$I_u = \frac{\sqrt{\overline{u^2}}}{\overline{U}} \tag{27}$$

where $\overline{u}$ is the deviation from the mean velocity $\overline{U}$.

The iso-surfaces indicates regions where large energy losses appears and contributes to the total drag. From the figure it can be noted that the wakes at the end of the cars is asymmetric due to the asymmetric design of the underbody. From Figure 26 it can clearly be seen that the wakes created at the rear wheels are interacting with the base wake, by prevent this interaction large improvements on the drag can be achieved. When comparing the sedan and wagon it's obvious that the largest difference is in the base wake. On the wagon separation occurs on the roof and can't be attached over the rear windscreen which it can do on the sedan model, this depends on the difference in angles over the rear windscreen.

Even though the exterior shape of the cars differ the greatest contribution to the drag will come from the same areas, the wheels, the underbody and the rear-end.

(a) Sedan (b) Wagon

Figure 26: Iso-surface for total pressure equal to zero, here coloured with turbulence intensity

4.1.2 Pressure and velocity

In Figure 27 the velocity magnitude at lateral location of $y=0$ is visible for the both models, as expected there is a high velocity region over the hood and the roof, and between these regions there are low speed regions with separated flow. According to *Bernoulli's equation,* Eq. (6), in regions with high velocities the pressure is low and separation might occur. These figures can be related to the previous figures showing the iso-surfaces, where low speed regions can be located in the base wake. By comparing Figure 26 and 27 it becomes obvious that the wagon has a higher drag coefficient, the wake is significant larger and the low speed region behind the vehicle is also greater then for the sedan model.

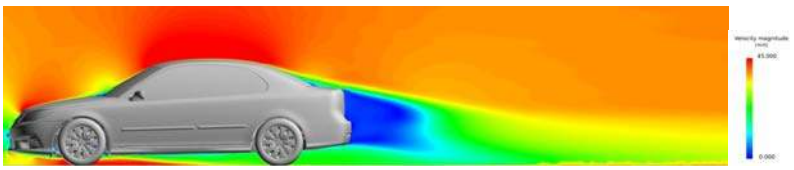

(a) Sedan

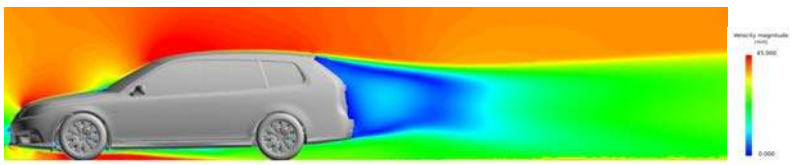

(b) Wagon

Figure 27: Velocity magnitude in $y=0$

By reducing the magnitude and shape of the wakes the total drag will be reduced, the focus in this study is to investigate the influence of the underbody design on the base wake. It's not only the magnitude of the wake that is influencing the total drag. The intensity of the flow also affects the resisting drag. In Figure 27a it can be seen that the flow in the wake is directed downward against the ground for the sedan model, this so called *downwash* is a source of drag and by balancing this wake

to a more streamline direction a lower drag can be achieved. To illustrate the direction of the flow in the wake Figure 28a has been made where the vectors indicates the direction of the flow. The wake can be seen as an extension of the car, a more streamlined wake will benefit the pressure recovery and hence reduce the drag. The downwash of the wake forces the flow underneath the car to flow around the wake area and expand the low-pressure region since the flow accelerates in proximity of the wake. The vectors shows a recirculation in the wake due to the higher speed from the air over the vehicle.

The high rake angle (see Section2.2.3) of the rear windscreen on the wagon will prevent the downwash and the same behavior can not be seen. In this model a more balanced wake can be noted which reduce the possibility to achieve an improvement of the same magnitude as for the sedan model.

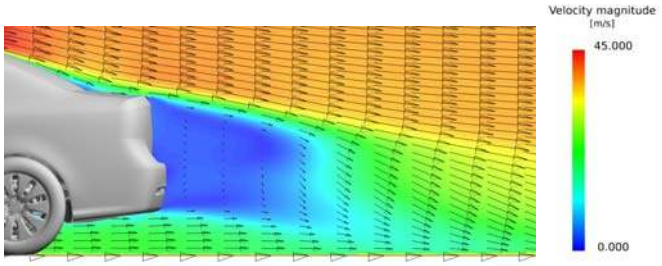

(a) Sedan

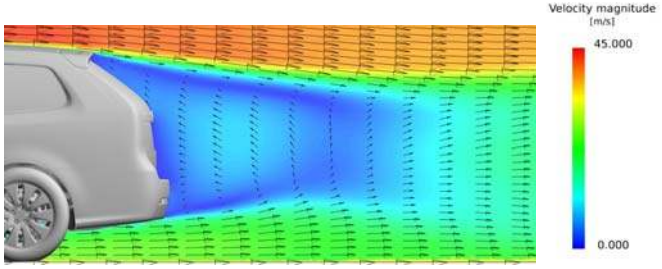

(b) Wagon

Figure 28: Velocity vectors in $y=0$ same velocity plane as before

4.1.3 Underbody analysis

Both the models has the same underbody structure and the same engine bay but the flow under the vehicles will have a different behavior. In Figure 29a the velocity magnitude is displayed at height of *0.1* meters above the ground to investigate the flow between the ground and vehicle. The red area in the front area in Figure 29a shows an acceleration of the flow and further downstream the flow decelerate which corresponds to earlier mentioned theory, this high velocity region can be derived from a change in ground clearence. The wakes behind the wheels that are shown in Figure 26 indicates region of high losses and influence on the base wake which also can be noted in Figure 29a. At a height of *0.32* meters above the ground it can been seen, see Figure 29b, how the base wake is expanding into two parts in the y-direction. This behavior can originate from the interaction with the rear wheels which indicates the large influence of the wheel design.

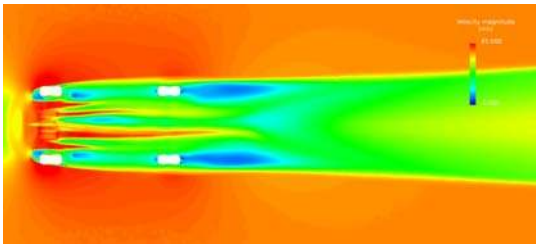

(a) *z=0.1 m*

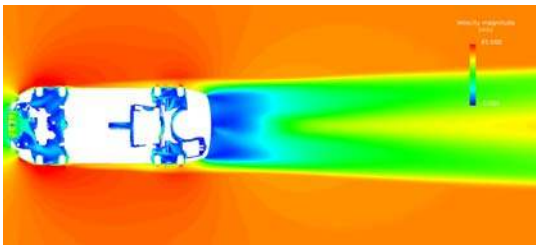

(b) *z=0.32 m*

Figure 29: Velocity magnitude in z-*planes* for the sedan

The difference between the sedan and wagon can be detected by looking at Figure 30 and compare the expansion of the wake in the y-direction. Meanwhile the sedan's wake is showing another behavior due to the stronger downwash which expands the wake in a lateral direction. Another reason for this behavior is that the wagon model has a more boot-tailed rear-end shape, see Section 2.2.3, which directs the flow inwards. It can also be noted in Figure 30 that the wheels has an major influence on the base wake (blue areas).

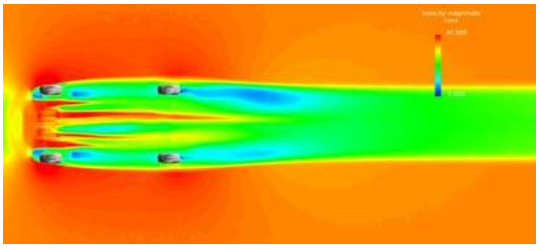

(a) *z=0.1 m*

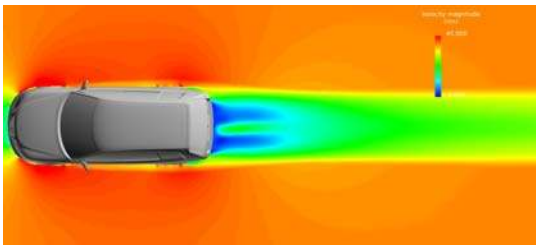

(b) *z=0.32 m*

Figure 30: Velocity magnitude in *z-planes* for the wagon

The wake propagation is illustrated in Figure 31 where the velocity magnitude is displayed in four different *x-planes*. There are three larger areas with lower velocities, the sides and in the middle by the exhaust system, these regions propagates downstreams and has an impact on the base wake. The figure also indicates the trailing vorticities created over the *c*-pillars.

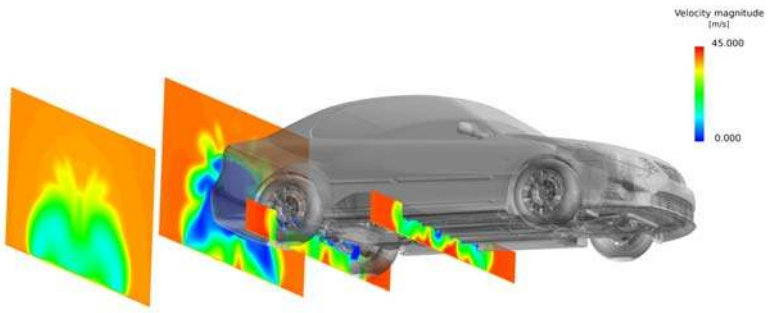

Figure 31: Velocity magnitude in *x=3.2; 4.5; 5.4 & 7 m*

Figure 32 visualizes a couple of streamlines released at the intake to the engine and shows that a great part of the flow leaves the engine bay underneath the vehicle, which indicates that a alteration of e.g. the pressure will affect the flow through the engine. The streamlines also indicates an irregular flow pattern at the rear-end as well as underneath the vehicle.

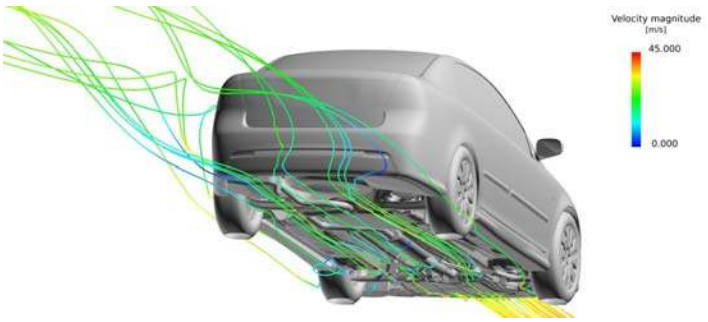

Figure 32: Streamlines through the engine bay to the underbody

4.1.4 Surface and pressure recovery

A major focus in this study is to investigate the wake and the pressure progression and in order to measure these properties images with the *pressure coefficient* (C_p) has been produced. Figure 33 visualizes the pressure coefficient on both models. At the sharp edges of the rear-ends it can be seen that C_p has a negative value, it's at these edges the flow will separate and create the low pressure wakes. In this study the pressure recovery of the vehicle is of great interest and an increase in the pressure coefficient on the trunk and the rear bumper is desired when implementing a diffuser. This increase in pressure at the rear part of the vehicle will reduce the effect of the *form drag* or *pressure drag*.

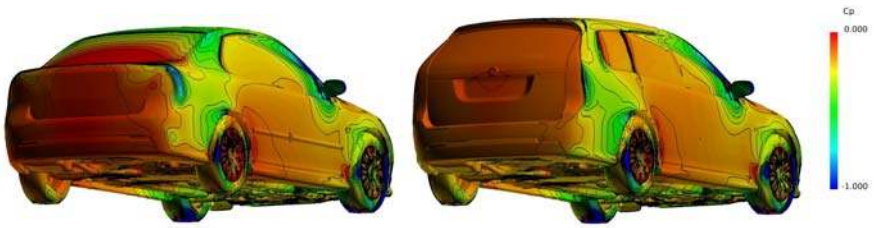

(a) Sedan (b) Wagon

Figure 33: Pressure coefficient for the reference models

Accumulated Drag An approach to investigate how the drag accumulates along the surface of the vehicle is to observe the accumulated C_d. The distribution of the drag can be seen in Figure 74 where the curve shows the drag forces above and under the vehicle which can be found in Appendix A.

4.1.5 Grid resolution

In Section 2.4.7 it was discussed if the computational grid was sufficiently resolved, one way to control this is to calculate the y^+ -value. In Section 2.4.4 y^+ is defined and a value between 30-300 indicates that the grid is sufficient to resolve the boundary layer. In regions where prism layers are not applicable

due to a lot of irregularities i.e. the underbody a value between 30-300 is hard to achieve. Figure 34 shows the y^+distribution of the wagon model with a random diffuser configuration to show that the values are within the limits. Red regions corresponds to a y^+ value of more then 300, this regions just occurs on sharp edges and it's almost impossible to avoid such regions. If there would have been some problems with a high y^+ -value the prism layers would have been reconfigured e.g. decrease the height of the first cell or implement a new prism layer, which was needed for the sedan model.

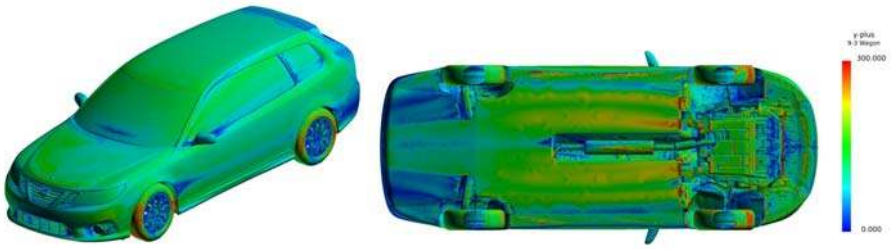

(a) Side (b) Diffuser

Figure 34: y^+ distribution on the 9-3 Wagon model

By investigating the growth of the boundary layer it's also possible to see if the mesh is refined enough, this is visualized in Figure 35. The sudden increase in velocity between the diffuser and ground depends on the rate at which the ground moves, as can be seen the profile rapidly increases to *38.89 m/s* which is the velocity of the ground.

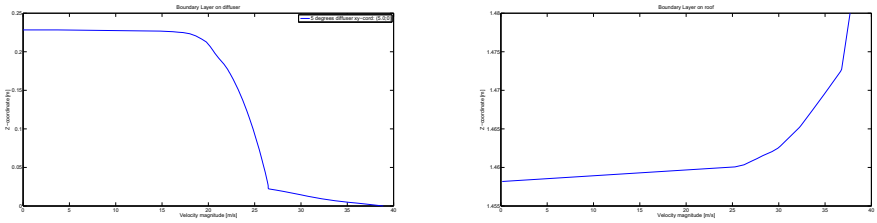

(a) Diffuser, *x=5* (b) Roof, *x=5*

Figure 35: Boundary layer growth in symmtery plane, *y=0*

4.2 Diffuser sweep

The diffuser angle is swept between three and 14 degrees in order to find a setup with the highest drag reduction.

4.2.1 Sedan model

The initial drag results from the simulations of the diffuser sweep of the sedan model can be viewed in Figure 36. These results shows that the setup with a *diffuser angle* (see Figure 16) around 8˚ degrees gives the best result in terms of low total drag. The results from these simulations also showed a

significant improvement in the drag relative to the reference case mainly due to the covering of the underbody.

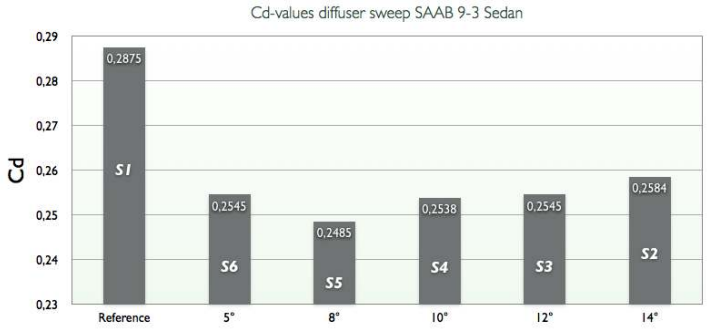

Figure 36: C_d-values for diffuser sweep on *SAAB 9-3 Sedan*

A closer study on the lifting force acting on the vehicle has been done and the results for the C_l values are shown in Figure 37. From this a correlation between the drag and lift force can be observed which indicates that an reduction in lift force has been achieved as well as an reduction in drag force.

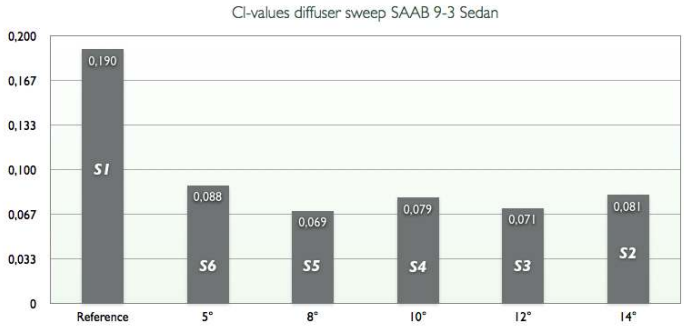

Figure 37: C_l-values for diffuser sweep on *SAAB 9-3 Sport sedan*

One of the main areas of interest is the pressure recovery which plays an key role in reducing the drag. In Figure 38 the pressure coefficient (C_p) is plotted on the surface for the reference case (*S1*) and the case with an 8° diffuser *(S5)*. The ambition is to increase the pressure in the rear in order to reduce the pressure difference between the front and rear part of the vehicle, a low pressure difference will result in a low pressure drag. Figure 38 shows how the pressure on the underbody with a diffuser progresses more smoothly than for the reference case and reduces the risk of separation.

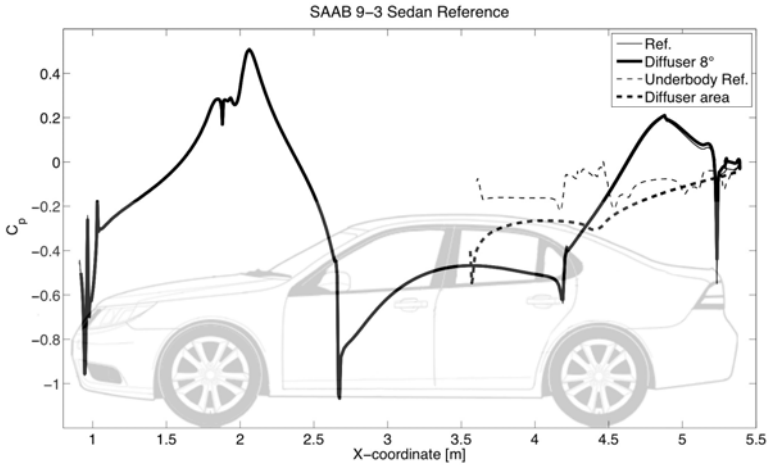

Figure 38: C_p plot in symmetry plane (y=0) *SAAB 9-3 Sport sedan*

An image of the entire rear region is shown to get an overview of the difference in surface pressure between the reference case and the one with an 8° diffuser, see Figure 39. In this image the function of the diffuser becomes more clear since an increase in the base pressure can be noted relative to the reference case. The colorscheme in Figure 39 is explained by the following points:

- green area: no change in C_p by implementing a diffuser
- red area: increase in C_p by implementing a diffuser
- blue area: decrease in C_p by implementing a diffuser

The main difference is that the diffuser increases the high pressure region in rear over a larger area and lower the total drag.

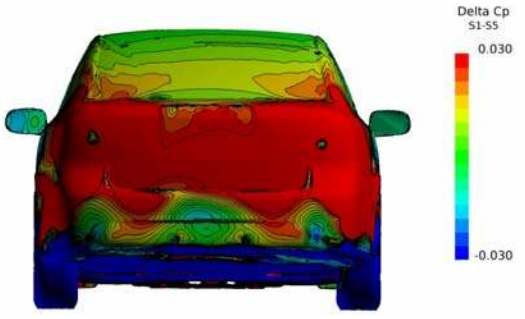

Figure 39: $\triangle C_p$ on *9-3 Sedan Reference & 9-3 Sedan 8° diffuser*

To measure how symmetric the pressure and flow is over the diffuser C_p-values has been extracted at a fix x-location of 0.4 meters from the rear bumper (x=5.0 m). The result is shown in Appendix

A Figure 75 and shows that the pressure is symmetrically distributed over the diffuser with a high pressure region in the center. This indicate that the flow is slowing down according to *Bernoullis equation* and the intended function is achieved.

A key parameter to reduce the drag of a vehicle is to streamline and balance the pressure wake behind the car. In Figure 40 areas of zero total pressure is displayed in order to visualize areas of high loss. Areas capsulated in this volume illustrates the wake structure and a comparison between the case with a 8° diffuser (*S5*) and the reference case (*S1*) shows the difference in length of the wake. This reduction in length can prove a reduction in total drag.

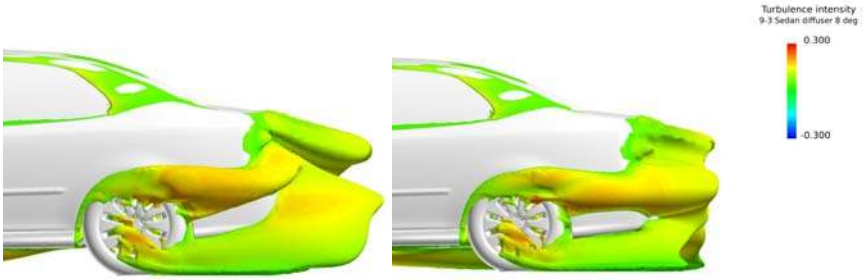

(a) Reference S1 (b) 8° diffuser S5

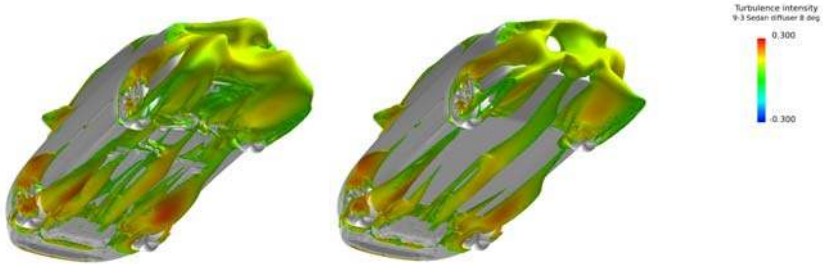

(c) Reference S1 (d) 8° diffuser S5

Figure 40: Iso-surface, *total-pressure=0, SAAB 9-3 Sedan*

Figure 40 also shows a reduction in losses under the vehicle due to implementation of the panels.

To further investigate how the wake structure is changed by implementing a diffuser coordinate planes in the *y-*, *x-*, *z-* direction have been made. The Figures 41-43 shows the velocity magnitude alteration between the reference case (*S1*) and the case with an 8° diffuser (*S5*). By introducing a diffuser it can be seen in Figure 41 that the wake (low pressure region) has shifted upward and decreased the downwash that existed in the reference case. Decreasing the downwash will streamline the wake and lower the overall drag, see Figure 36.

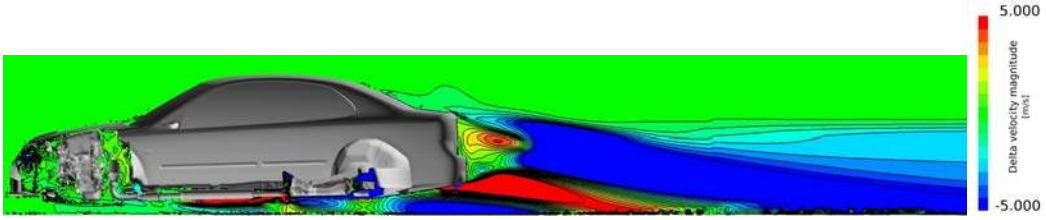

Figure 41: $\triangle V$-plot velocity magnitude in symmetry plane (y=*0* [m]), *S1-S5*

By taking a closer look at the velocity change in a z-plane reveals that the wake is more streamline or narrow in the case where a diffuser (*S5*) was used, see Figure 42. This is mainly due to the fact that the pressure has been increased around the sides of the rear bumper, see Figure 39.

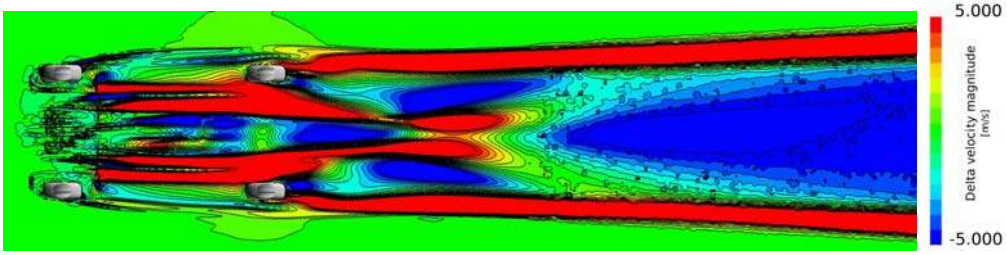

Figure 42: $\triangle V$-plot velocity magnitude in z-plane (z=*0.1* [m]), *S1-S5*

A series of x-plane was created to show how the flow progresses downstream, see Figure 43. The figures shows regions of increased and decreased velocity when introducing a diffuser, green area means no change, red area indicates an increase in velocity and blue area a decrease. At a location in the center of the rear wheels (x=*4.5 [m]*) a $\triangle$-plot of the velocity magnitude shows an increase in velocity under the vehicle which indicates a rise in downforce. Further downstream it becomes more clear that there has been a successful pressure recovery (x=*7.0[m]*), large red areas.

(a) x=*4.5* [m] (b) x=*5.4* [m] (c) x=*7.0* [m]

Figure 43: $\triangle V$-plot velocity magnitude in z-planes, *S1-S5*

To establish if an implementation of a diffuser will influence the overall vehicle dynamics in terms of handling a study on the pitch moment was done. In Figure 44 the results from this investigation

are shown and the pitch of the vehicle is expressed with the coefficient of moment, C_m. The original reference model shows a C_m value that indicates a diving pitch moment and by introducing a diffuser this behavior has been decreased. It should be noted that the alteration are slight and a serious impact on the handling can not be observed.

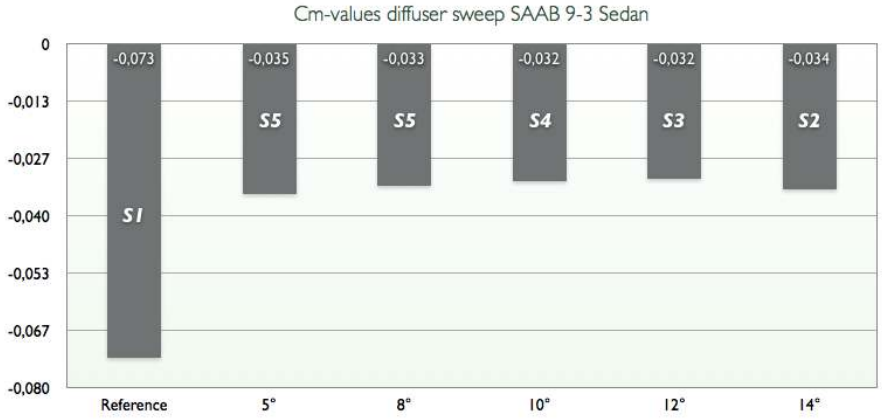

Figure 44: Coefficient of moment, C_m, *SAAB 9-3 Sport* sedan

4.2.2 Wagon model

The drag results form the unmodified *SAAB 9-3 Sports wagon* model showed that it had a higher C_d-value than the *SAAB 9-3 Sport sedan* model. In Figure 45 results from the diffuser sweep on the wagon model are shown which indicates that the most effective setup was found in case *W6* (5° diffuser) in terms of lowest C_d-value. But the improvement is not substantial relative to the reference model (*W1*) and the difference in drag between each diffuser setup is not large. This means that the reference wagon (*W1*) has lower potential for drag reduction than the reference sedan (*S1*).

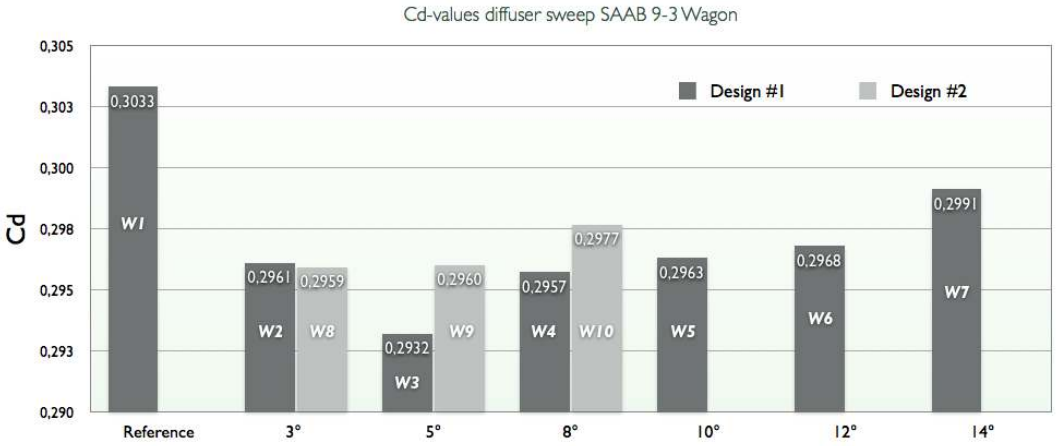

Figure 45: C_d-values for diffuser sweep on *SAAB 9-3 Sport wagon*

A closer study on the lift force acting on the wagon model has been done and the resulting lift coefficient, C_l, values are shown in Figure 46. A correlation between the drag and lift force can be observed that shows a clear increase in downforce by implementing a diffuser and a reduction in drag. The case *W9* with a *5°* angled diffuser shows the highest downforce and also a relative low C_d can be noted in Figure 45, a closer look at this case has been done in this section.

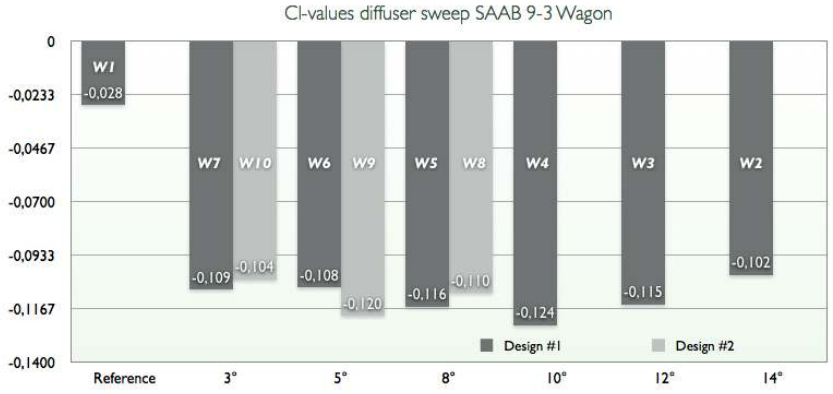

Figure 46: C_l-values for diffuser sweep on *SAAB 9-3 Sport wagon*

The function of the diffuser is to increase the base pressure and in Figure 76 which can be found in Appendix A shows a plot is with the pressure coefficient (C_p) on the surface for the reference case and the setup with a *5°* diffuser (*W9*). From this figure it could be concluded that the pressure builds up in a smoother way when a diffuser is implemented which also was observed for the sedan model.

To investigate the pressure at the surface in a more visible manner Figure 47 was made to shows the difference in surface pressure between the reference wagon case (*W1*) and the case with an *5°* angeled

diffuser (*W9*). The colorscheme in Figure 47 is explained by the pointlist in the previous section.

It can be observed that the center of the rear trunk has a decrease in pressure but in areas around the center of the trunk the pressure recovery is significant which results in an decrease in drag.

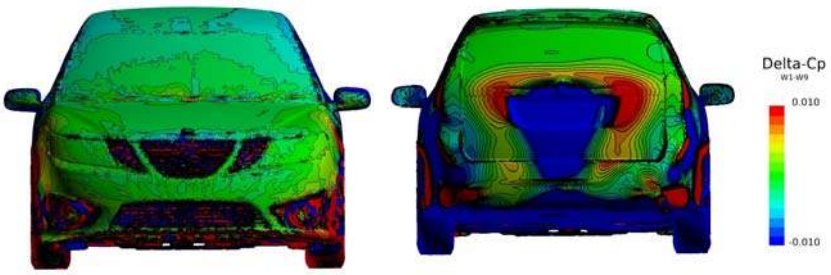

Figure 47: $\triangle C_p$ on rear-end between *9-3 Wagon Reference* and *9-3 Wagon 5° diffuser*

The undercarriage and engine bay is not symmetric which results in an asymmetric flow and by plotting the pressure coefficient at a fix x-location on the diffuser the effect of this can be investigated. In Appendix A Figure 77 shows that the pressure is not symmetric along the diffuser in a lateral direction.

As mentioned in Section 4.1 the pressure wake's distribution and shape will influence the total drag. A Sportwagon's characteristic box shape will cause the wake to have a different appearance compared to the notch shaped sedan model. The separation of the flow originates from the roof-edge which results in a large pressure wake at the rear part of the vehicle, see Figure 48. By comparing the side view in Figure 48 there is a clear difference in shape but not size. A closer look at the underbody and wake indicates that the diffuser increased the pressure in the lower middle of the wake and lowered the total pressure in the upper part of the wake. A major difference can be noted under the vehicle where the losses appeared to be lower due to the smoother underbody.

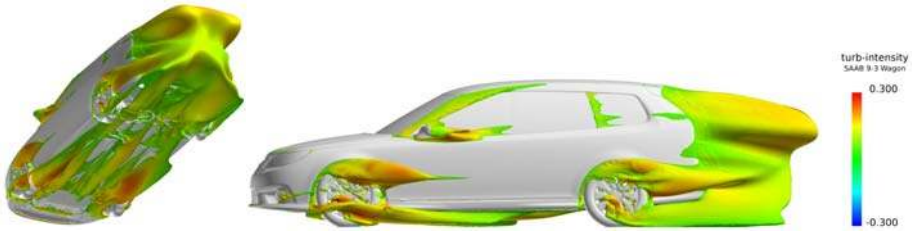

(a) Reference

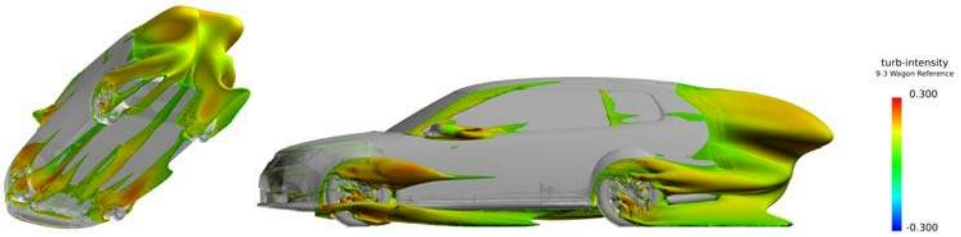

(b) 5° Diffuser

Figure 48: Iso-surface *SAAB 9-3 Stationwagon*

One way of showing the impact of using a diffuser is to compare the velocity magnitude in △-plots, see Figures 49-51. These figures shows the difference in flow field velocity between the reference case (*W1*) and the case with an 5° diffuser (*W9*). In Figure 49 it is clear that there has been an increase in velocity magnitude (red area) after the vehicle near the ground. An increase in velocity will give a reduction in total pressure (dynamic and static pressure). It can also be observed that in this fix y-location the wake has been forced upward due to the diffuser.

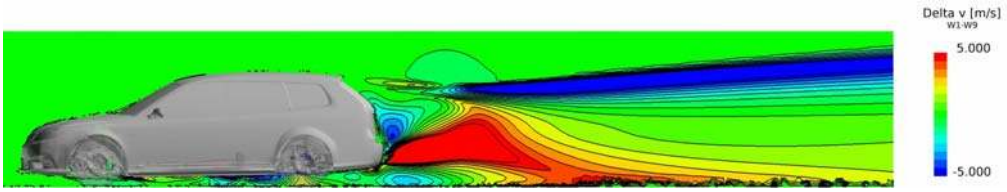

Figure 49: $\triangle V$-plot velocity magnitude in symmetry plane (y=*0* [m]), *W1-W9*

At the location *z=0.1 [m]* a plane with the difference in velocity magnitude has been plotted in Figure 50. The figure shows how the diffuser affects the velocity of the air flow by increasing the speed of the air and making the wake more narrow in the y-direction. This increase in velocity (red area) will give a lower pressure, Figure 50 also shows a decrease in air motion after the rear wheels which will result in improved pressure recovery.

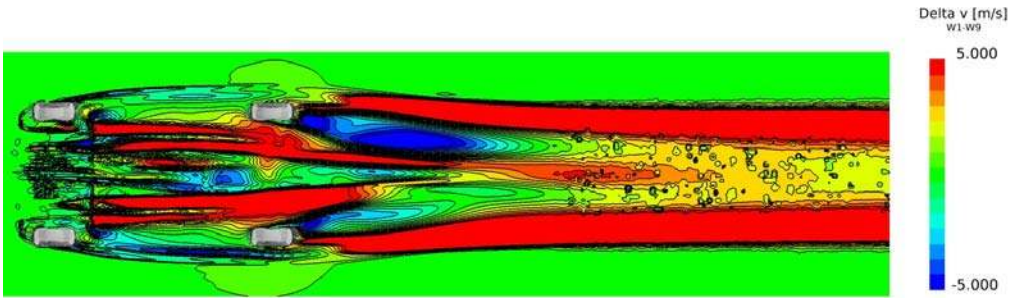

Figure 50: $\triangle V$-plot velocity magnitude in z-plane (z=*0.1* [m]), *W1-W9*

To investigate alterations in velocity and pressure further the velocity magnitude was potted in three planes in the x-direction, see Figure 51.

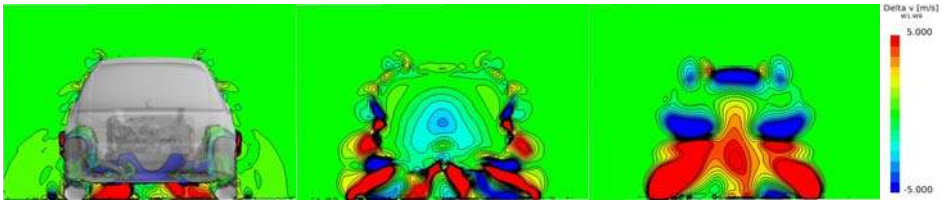

(a) x=4.5 [m] (b) x=5.4 [m] (c) x=7.0 [m]

Figure 51: $\triangle V$-plot velocity magnitude in x-plane, *W1-W9*

These figures shows how the wake area progresses downstream and the difference between the two cases. By implementing a diffuser the lower pressure region or wake which is the source of the pressure drag will be push up in the z-direction. A re-direction of the wake can result in an upwash and make the low pressure region less streamline and then increase the total drag. In this case the increased upwash did not have a large impact on the total drag due to the covering panels on the underbody. This statement indicates that the covering panels has a larger impact on improving the aerodynamics than the diffuser it self.

In Figure 52 the result from the pitch moment investigation can be found which shows that the influence of using a diffuser increases the normal forces on the rear wheels. The increase normal force on the rear wheels is slight which will not effect the handling significant.

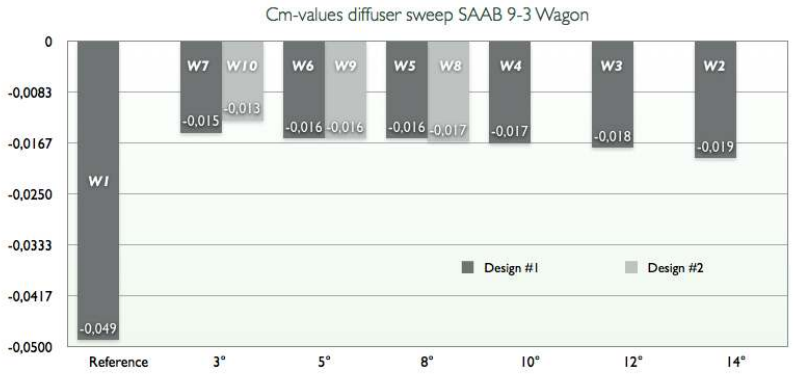

Figure 52: Coefficient of moment, C_m, *SAAB 9-3 Sport wagon*

4.2.3 Force analysis

A drag reduction has been establish by observing the C_d-values in Figure 36 and 45, to confirm this a force analysis has been done. This shows that the forces acting of the car body and rear bumper has been decreased and a reduction in resisting drag forces is achieved by implementing a diffuser, see Table 6.

Table 6: x-forces on selected parts

Case	Car body [N]	Rear bumper [N]	Total [N]
S1	13.7	-	13.7
S5	-31.6	-	-31.6
W1	-80.8	95.6	14.8
W9	-79.7	76.3	-3.4

4.2.4 Radiator flow

A vital aspect of vehicle aerodynamics is the air flow through the radiator and by adding a diffuser the pressure under the car change and affect the flow through the engine bay. In Figure 53 the massflow through the radiator is shown which indicates a lower massflow rate when adding a diffuser. This behavior is contradicting since the lower pressure created under vehicle by the diffuser would suck the air through the radiator.

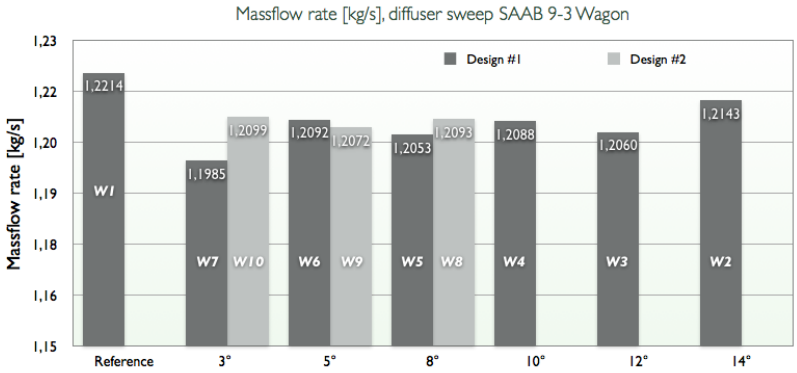

(a) *SAAB 9-3 Sport wagon*

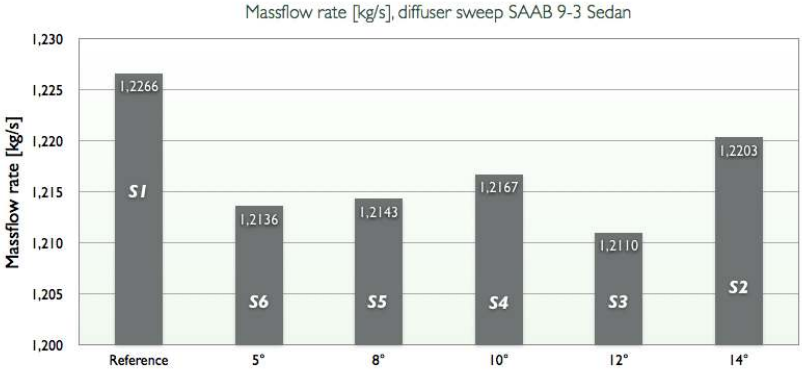

(b) *SAAB 9-3 Sport sedan*

Figure 53: Massflow rate trough the radiator

To investigate this behavior an image of the total pressure difference between the reference case (*W1*) and the case with a diffuser (*W9*) was created. Figure 54 indicates a pressure rise in the engine bay but also a pressure decrease in the front air intakes which indicates a local velocity increase.

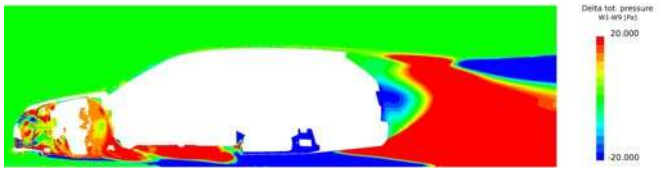

(a) Y-plane at *y=0.1* [m]

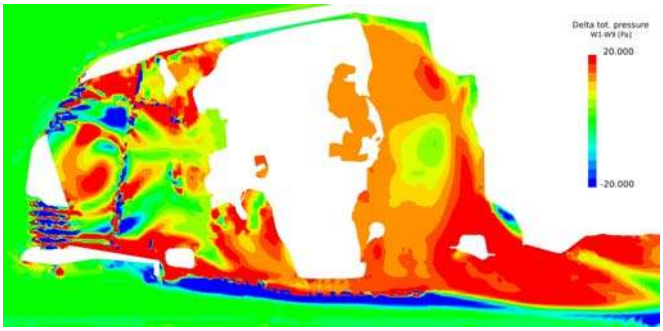

(b) Y-plane at *y=0.1* [m], zoomed image of engine bay

Figure 54: Difference in total pressure between *Reference wagon (W1)* and case *W9*

The reason for the higher pressure inside the engine bay when introducing a diffuser can be derived from the increased pressure at the beginning of the cover plates (behind the front wheels). To reduce this increased pressure a redesign of the interface between the underbody and coverpanels can be done. An image of the total pressure in the radiator is shown in Figure 55 that indicates an increase and decrease of the pressure in different areas in the radiator. This irregular change in pressure between the two cases shows that a different approach to model the radiator should be done in order to draw any distinct conclusions.

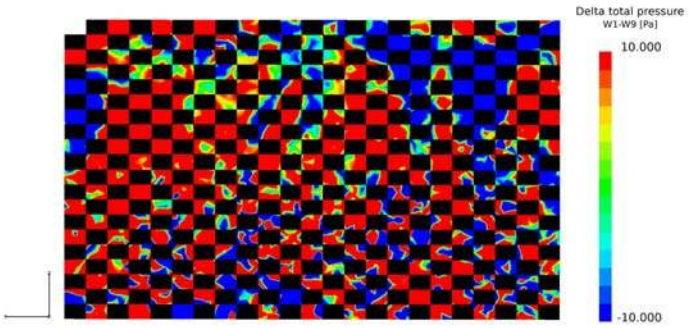

Figure 55: Difference in total pressure between *Reference wagon (W1)* and case *W9* in the radiator

4.3 Additional drag reduction devices

The analysis of the diffuser sweep showed that an efficient drag reduction angle of the diffuser could be found both for the *SAAB 9-3 Sport sedan* and *SAAB 9-3 Sports wagon*. By implementing different additions to the diffuser an even more effective diffuser could be achieved. The different drag reduction devices was describe in Section 3 together with the expected effects. During the diffuser sweep it was found that a diffuser angle of 8° gave the highest drag reduction for the *Sedan* and 5° for the *Wagon* which gave a starting point for improvement.

4.3.1 Guiding vanes

The purpose of using *vanes* in a diffuser is to direct the flow in the direction of motion and shield the flow under the vehicle from lateral wind gusts. An introduction of *guiding vanes* can direct the flow and decrease the turbulent effects from the rear wheels. In Figure 56 results from different configurations with guiding vanes are presented. The abbreviations in the figure corresponds to the test matrix, see Table 3. The trend is obvious, the introduction of guiding vanes has a positive impact on the lift, but a slight increase in drag.

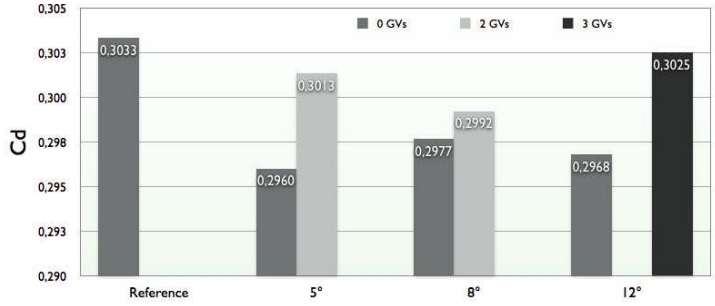

(a) Wagon

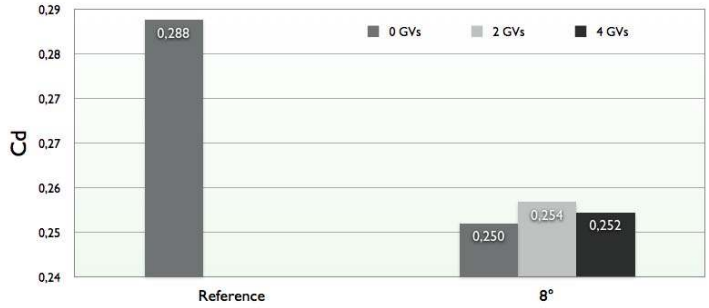

(b) Sedan

Figure 56: Drag coefficient results with guiding vanes

By looking on the x-forces acting on these cases, see Table 7, it can be concluded that the introduction of guiding vanes increases the resistance force on almost all parts. A distinct correlation between the diffuser and underbody can be noted which indicates that there exists a balance between them and that it can be controlled by introducing guiding vanes. Further investigation and new simulations can result in a setup with guiding vanes that has a net positive effect that are not achieved with these setups.

Table 7: x-force comparison, with and without guiding vanes

(a) Sedan

	S5 [N]	*S7* [N]	△*S7-S5* [N]	*S9* [N]	△*S9-S5* [N]
Diffuser	27.2	28.4	+1.2	28.3	+1.1
Car body	-31.1	-27.8	+3.3	-30.0	+1.1
Rear wheels	32.9	34.6	+1.7	35.2	+2.3
Rear suspension	6.3	6.4	+0.1	6.5	+0.2
Underbody	-58.7	-60.0	-1.3	-57.3	+1.4
TOTAL	-23.4	-18.4	+5.0	-17.3	+6.1

	W9 [N]	*W12* [N]	*W12-W9* [N]	*W8* [N]	*W11* [N]	*W11-W8* [N]	*W3* [N]	*W13* [N]	*W13-W3* [N]
Diffuser	46.9	55.1	+8.2	51.4	48.4	-3.0	54.0	58.1	+4.1
Car body	-79.7	-78.4	+1.3	-80.4	-79.1	+1.3	-81.1	-79.2	+1.9
Rear bumper	76.3	78.2	+1.9	76.2	76.4	+0.2	75.8	77.3	+1.5
Rear wheels	43.7	45.5	+1.8	43.7	44.6	+0.9	42.2	42.2	±0
Rear suspension	7.0	7.4	+0.4	7.4	7.4	±0	7.5	7.2	-0.3
Underbody	-52.8	-53.1	-0.3	-52.9	-49.8	+3.1	-49.9	-50.3	-0.4
TOTAL	41.4	54.7	+13.3	45.4	47.9	+2.5	48.5	55.3	+6.8

(b) Wagon

In Figure 57 an image of the difference in velocity magnitude between case *S5* and *S9* has been done which shows an alteration in velocity due to the introduction of the vanes. It can now be noted that the flow onto the vanes has an angle which results in an induced drag and an asymmetric separation over the vanes. A reason for this asymmetric flow onto the vanes can be derived from the design of the underbody. Figure 57 also shows a distinct influence on the flow upstreams due the introduction of the guiding vanes which is noteworthy. This influence on the flow upstreams can affect the entire flow field around the vehicle, such as the air flow through the rims. The introduction of the guiding vanes not only effects the flow downstream, changes in velocity and pressure can be noted upstreams which can be derived from the guiding vanes. The flow can either be sucked or pushed under the vehicle and move the stagnation pressure.

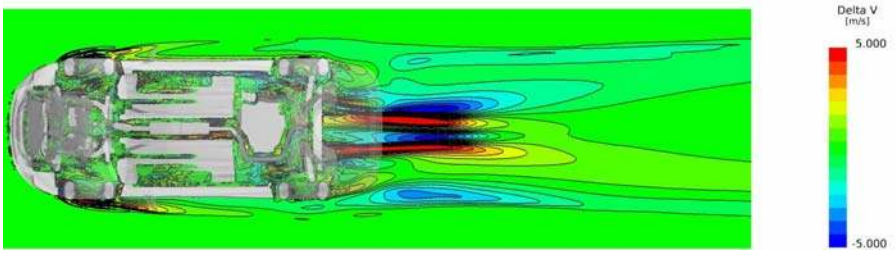

Figure 57: Change in velocity field in *z=0.2*, *S9-S5*

To study the increase in force on the car body a pressure investigation was performed. In Figure 58 an image of the pressure coefficient has been produced to investigate the affect of the alteration of the flow upstreams and the pressure alteration on the rear. A significant change in the stagnation point in the front can be observed which can explain the increase in drag when implementing guiding vanes. The stagnation pressure has been moved down and affect the in- and out-flow to the engine bay which clearly affect the flow around all the wheels.

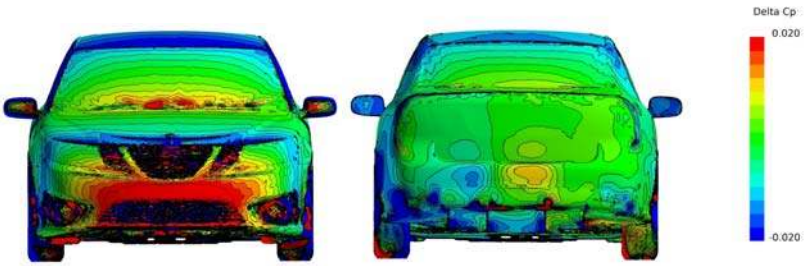

Figure 58: Alteration in pressure coefficient, *S9-S5*

In order to make a successful implementation of guiding vanes a further investigation on the flow onto the diffuser must be done to conclude the affect of the flow symmetry. To achieve a successful implementation of guiding vanes a redesign of the underbody has to be done, with more covering panels which results in a more symmetric flow and funnel the flow in the intended way.

A case with three guiding vanes directed outwards was simulated with the intended function to expand the air in a lateral direction and alter the behavior that could be seen in Figure 57. In Figure 59 the result from this can be seen and shows that this was not achieved and an increase in force on the diffuser could also be noted for this configuration. A rise in stagnation pressure could not be observed on this configuration due to the more symmetric flow.

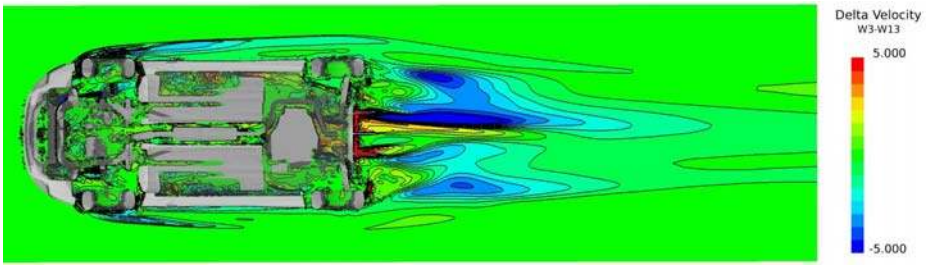

Figure 59: $\triangle V$ in *z=0.2* with directed vanes, *W13-W3*

4.3.2 Vortex generators

The aim with the implementation of *vortex generators* is to get a reattached flow and thereby improve the pressure recovery function. As separation is more predominate with a diffuser that has a higher angle the configurations of the cases with vortex generators had diffuser angles of 8 and 12 degrees. Results from the simulations showed that the largest improvement could be found on the wagon model with an 8 degree diffuser. The theory for using vortex generator may appear simple and straight forward but in practical it is difficult to achieve a re-attached flow since the variables are numerous. In Figure 60 the drag coefficient results for the cases with vortex generators are presented, and in Table 8 the force reduction in the x-direction is shown. From the table a reduction in resisting force can be noted for the wagon model, the force reduction can not be derived from a single region of the vehicle. It is rather a sum of small improvements in the flow field around the car.

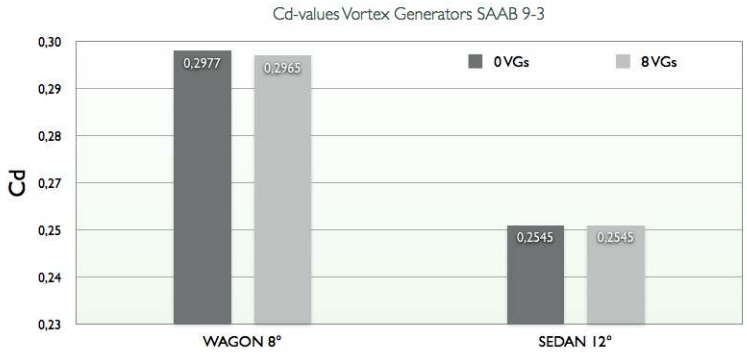

Figure 60: Drag coefficient results for the vortex generators

Table 8: $\triangle x$-*forces* with vortex generators

Case	Force [N]
S10-S3	6.1
W14-W8	-2.7

Since an improvement could be noted for the wagon model in terms of drag a further investigation was done to explain the reason for this improvement. An explanatory approach is to observe the velocity difference between the case with and without vortex generators with the same diffuser angle. Figure 61 initial shows an irregular behavior which indicates some transient behavior, see left front wheel. This means that a steady-state simulation is not enough to make a concluding remark. With this mentioned an improvement has been done but the source of the drag reduction can not be established.

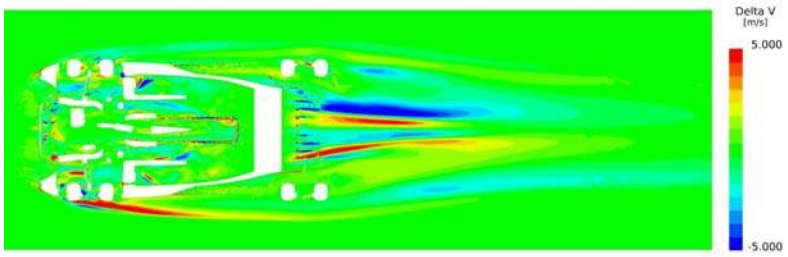

Figure 61: $\triangle$velocity magnitude in *z=0.25*, *W8* and *W14*

The attached flow generated from the vortex generators can also be visualized in Figure 62, which shows that the flow is attached longer on the diffuser and generate a higher upwash of the flow. In Appendix A an image of the streamlines from behind can be found which shows a concentration of the upwash in a y-direction when implementing vortex generators.

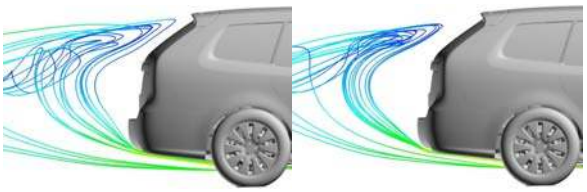

(a) With VGs (b) Without VGs

Figure 62: Streamlines comparison of the vortex generators

To verify the intended function of creating induced vortices and increase the momentum of the flow a pressure investigation can be done on the surface of the diffuser. In Figure 63 the pressure coefficient is displayed which indicates a low pressure area behind the vortex generators and a high pressure before them. This observation can prove that small scale vorticies are achieved and provides an increase in momentum to the flow.

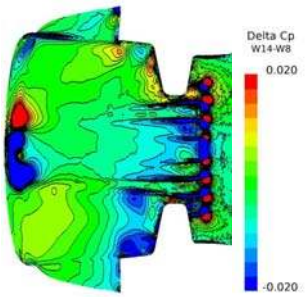

Figure 63: Pressure coefficient variation with and without vortex generators

To investigate the flow separation Figure 64 shows the *wall shear forces* and a value below zero indicates separation, the results shows that a larger area is attached with the vortex generators. This result indicates that a higher magnitude of attached flow improves the drag reduction.

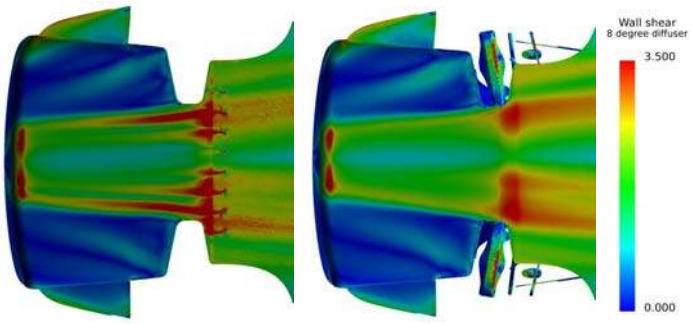

(a) *W14* (b) *W8*

Figure 64: Comparison of wall shear, τ_ω

4.3.3 Covered wheels

A large amount of effort has gone into different the rim designs the latest few years with the ambition to minimize the drag. In this study the rear rims has been sealed and simulations with all four rims covered has been performed, see the results in Figure 65.

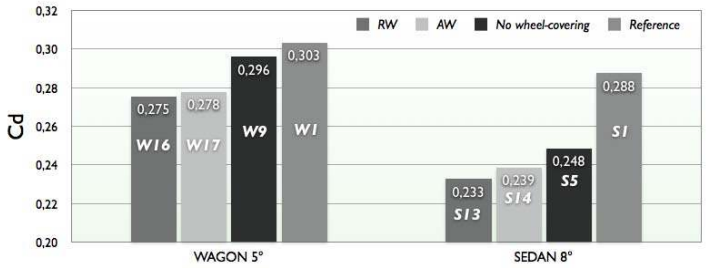

Figure 65: Drag coefficient results for the covered wheels

A large contribution to the total drag is the wake creation around the wheels, these wakes influence the flow under the vehicle and hence the base wake. One way to influence this flow is to cover the rims so no air will be sucked through the rims and disturb the flow under the vehicle, a reduction of the pressure wake on the wheels it self can be noted. In Figure 66 iso-surfaces from the simulation with the rear wheels covered is shown, in Appendix A images of the case with all wheels covered can be found. In both configurations the wakes are reduced compared to the reference case, especially around the rear wheels which leads to a smaller base wake.

(a) From behind (b) From below

Figure 66: Iso-surface comparison between *S1*-*S13*

From Figure 65 it was determined that the highest drag reduction was achieved with covered rear wheels. To explain this result an analysis of the forces acting on the rear wheels was done, see Table 9. It can now be determined that the covering of the front wheels will guide the flow straight on the rear wheels and increase the stagnation pressure on rear wheels, i.e. higher force value.

Table 9: *x-forces* on rear wheels

Case	x-force rear wheels [N]
S1	29.1
S13	33.8
S14	47.1

A configuration with the front wheels covered was not prepared due to knowledge that a covering of the front wheels will lower the drag force but not to the desired extend as covering the rear wheels. Covering only the rear wheels will benefit the base pressure more then covering both front and rear wheels, due to the changed underbody flow propagating from the front wheels.

This design of rims when the wheels are sealed of entirely is not realistic since the air flow through the rims is needed to cool the brakes. *Volvo Car Cooperation* (VCC) has made CFD calculations on this problem and have designed rims that is passing through sufficient air to cooling the brakes and still lowers the drag.[15]This approach is something that would be of interest for *SAAB Automobile* especially when introducing a diffuser when these results indicates a large improvement.

The reason for increased drag with covering on both the front and rear wheel can depend on the increased pressure in the front wheelhouse. The outflow from the wheel house will be more significant with higher velocities then with a normal ventilated rim.

Figure 67 shows the differences in C_p between case with and without covered wheel and an 8° diffuser. According to [15] an increase in base pressure should be noted when covering the rear wheels. In the case with covered rear wheels it's clear that the base pressure is increased more then with all wheels covered. It could also be noted that the sides of the rear trunk is clearly affected and improves the pressure recovery in a lateral direction. An asymmetric behavior can be noted in the figures which depend on the design of the engine bay that demonstrates how important the design of the engine bay becomes when covering the wheels. A similar behavior could be noted for the wagon model which do not require a detail analysis without being redundant.

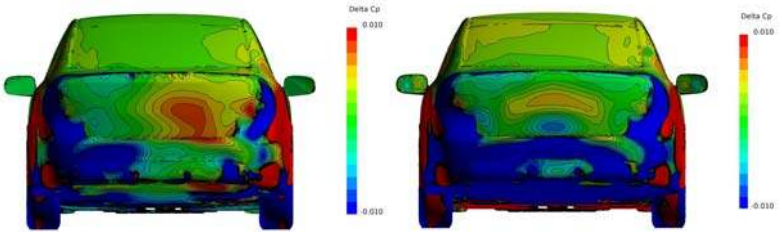

(a) Covered rear wheels (b) Covered front and rear wheels

Figure 67: Pressure coefficient difference for the different rim configurations

4.3.4 Covering of rear suspension

Figure 68 shows the results for the configurations with covering of the rear suspension. When analyzing the diffuser sweep it was found that the gap for the rear subframe generated a turbulent flow. By cover this area a less turbulent flow would be achieved which should lead to more attached flow on the diffuser. This redesign of the covering panels and diffuser required a modification of the rear suspension.

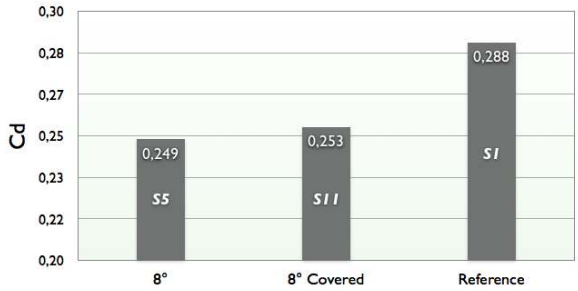

Figure 68: Drag coefficient results for covering of the rear suspension

An expected result from this simulation was that the drag should decrease but instead an increase in drag could be noted. The magnitude of the increase in drag is not significant but confusing. To resolve this issue an analysis on the forces acting of the vehicle was done. In Table 10 an increase of the force acting on the car body could be noted which indicates that the pressure recovery did not improve.

Table 10: x-forces on the diffuser

	S5 [N]	*S11* [N]	*S11-S5* [N]
Diffuser	27.2	30.3	+3.1
Car body	-31.1	-24.2	+6.9
Rear wheels	32.9	32.8	-0.1
Rear suspension	6.3	3.3	-3.0
Underbody	-58.7	-59.5	-0.8
TOTAL	-23.4	-17.3	+6.1

In Figure 69 iso-surface of total pressure equal zero is visualized for both cases, the red surface is the old diffuser and the blue is the diffuser with covering of the rear suspension. From this picture is is obvious that the losses has increased from the rear wheels but improved under the diffuser.

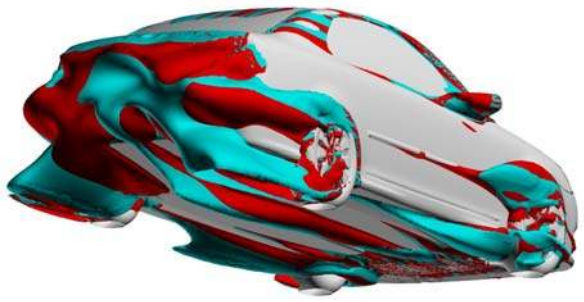

Figure 69: Iso-surface comparison with flat underbody

To investigate this alteration in behavior around the wheels and the ability to regain the pressure in the rear (pressure recovery) two pictures of C_p is presented in Figure 70. The images shows a reduction in pressure on the rear surface which explains the increase in drag it also shows how the pressure on the wheels has been altered. The modification on the diffuser appear to have increased the pressure inside the wheels and increased the pressure on the rear rims. This reveals an alteration of the flow through the wheels that affects the pressure recovery in a negative way.

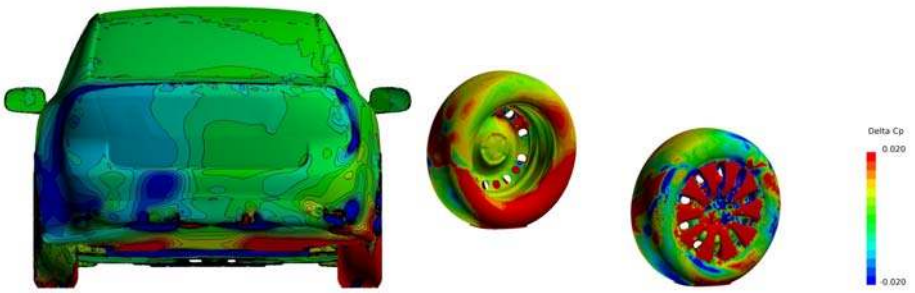

Figure 70: Pressure coefficient difference between *S5-S11*

4.3.5 Only diffuser

In all simulated cases the diffuser has been fused together with the cover-panels and to establish the cover-panels affect two simulations with no panels was simulated. The results from these simulations can be seen in Figure 71. By removing the covering-panels the flow characteristics has been changed before it reaches the diffuser, and the higher degree of turbulence will obstruct the flow to attach on the diffuser surface.

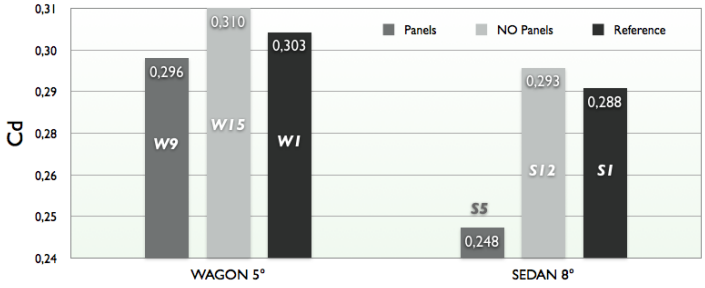

Figure 71: Drag coefficient results without cover panels

It should be noted that the design of the diffuser differ between the wagon model and the sedan model. The design of the diffuser on the sedan model had an expected result since there exists a gap between the underbody and diffuser that acts as an airbrake. On the other hand the diffuser on the wagon model had been designed to solve existing problems on the diffuser from the sedan model. The result for the wagon model did not either meet expectation on lowering the drag relative to the

unmodified reference model. A conclusion could be made that the panels has a great influence on the diffuser.

In Table 11 the x-forces for related surfaces are presented, as can be noted there is a significant increase in resistance forces for both models. On the sedan model the largest alteration was located on the car body, i.e. the pressure recovery had been deteriorated due to the removal of the panels. The rear subframe that has been covered by the panels also increased the resisting force due to the new design, and especially for the wagon model.

Table 11: x-forces case for *S5, S12, W9 & W15*

(a) Sedan

	S5 [N]	*S12* [N]	*S12-S5* [N]
Diffuser	27.2	29.6	+2.4
Car body	-31.1	13.9	+45.0
Rear wheels	32.9	39.6	+6.7
Rear suspension	6.3	17.1	+10.8
Underbody	-58.7	-60.1	-1.4
TOTAL	-23.4	40.1	+63.5

(b) Wagon

	W9 [N]	*W15* [N]	*W15-W9* [N]
Diffuser	46.9	58.6	+11.7
Car body	-79.7	-78.0	+1.7
Rear bumper	76.3	77.9	+1.6
Rear wheels	43.7	46.5	+2.8
Rear suspension	7.0	26.5	+19.5
Underbody	-52.8	-71.2	-18.4
TOTAL	41.4	60.3	+18.9

The most interesting area is the underbody since it's where the modifications have been done, in Figure 72 the pressure coefficient differences is presented for the wagon. Similar images on the sedan can be found in Appendix A Figure 79. As can be seen there is an increase in pressure around the rear suspension and the interface between the diffuser and underbody which explains the increase in drag value. The figures also indicates the importance of the covering panels which improves the pressure recovery and hence the aerodynamic resistance. This is even more clear on the sedan where the pressure coefficient decreases over the rear without the panels.

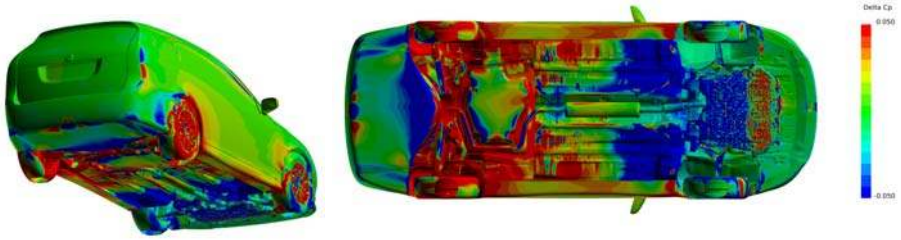

(a) Side view (b) Under

Figure 72: Pressure coefficient difference *W15-W9*

The unmodified sedan model showed an downwash that effected the resisting drag force, when removing the cover panels the diffusers couldn't mange to direct the flow upwards and streamline the wake see Figure 73.

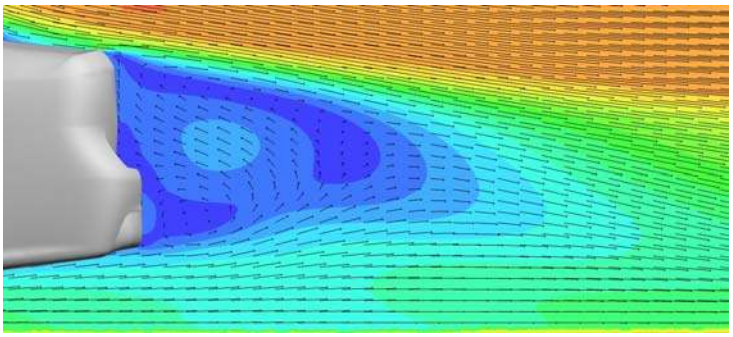

(a) *S5*

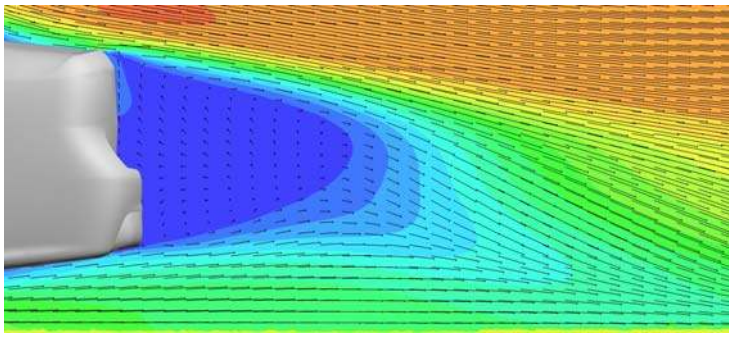

(b) *S12*

Figure 73: Velocity vectors that indicates the downwash in *y=0*

4.4 Fuel consumption

There is a standard procedure for calculating the fuel consumption for new passenger cars entering the market. This is done by driving the vehicle in a standard driving cycle that should correspond to a normal use of a car, in this case the *New European Driving Cycle* (*NEDC*) is used. The simulation can either be performed in a roller test bench or, as in this case, simulated with a computer. *SAAB Automobile* have done simulations with the new drag coefficient values and results for the fuel consumptions are presented in Table 12. As can be seen the reduction in fuel consumption is not as large as the reduction in drag coefficient due to the fact that the largest part of the *NEDC* is performed at lower velocities.

Table 12: Improvement in fuel consumption between the references cases and the cases with covered rear rims

(a) Sedan

	Fuel consumption	Drag coefficient, C_d
S1	7.76 [l/100km]	0.288
S13	7.57 [l/100km]	0.233
$\triangle$ [%]	-2.5	-19.1

(b) Wagon

	Fuel consumption	Drag coefficient, C_d
W1	7.9 [l/100km]	0.303
W16	7.8 [l/100km]	0.275
$\triangle$ [%]	-1.3	-9.25

5 Conclusions

The motivation for this study is to discover a clear trend by implementing a diffuser in order to reduce the resisting drag force. A trend is investigated by observing the pressure at the rear end of the vehicle and increasing the pressure recovery by altering the wake structure. To determine significant flow field alteration by altering the geometry images that combine results from different configurations has produced which are called *delta figures*. With these figures together with numerical data results the following number of concluding points has been drawn.

- Convergence of the results has been achieved but an asymptotic solution is not fulfilled. This means that the trend is established but the numerical values can differ when using a different computational grid on the same cases.
- Results from the simulations on the unmodified model of the *SAAB 9-3 Sport sedan* and *SAAB 9-3 Sports wagon* showed that the wake structure on the sedan model had larger potential for drag reduction.
- The flat panels places over the underbody together with a diffuser with an sloped angle of 8° showed the best improvement on the sedan model. This setup contributed to a smooth increase in pressure without any separation and a better pressure recovery than the unmodified sedan model.
- A similar trend could be noted on the wagon model but in this case the unmodified wagon model gave a balanced wake structure and an improvement could be noted by only flattening the existing underbody. This result indicated that the a diffuser with a sloped angle of 5° showed the best improvement in C_d.
- The lifting force has a significant impact on the handling of the vehicle on both model a decrease in lifting force was noted due to the panels and diffuser that contributed to increase in ground effects. The pitching moment was not heavily disturbed by the new geometry of the underbody.
- A significant improvement could be noted by covering the rear wheels which shows a great relation between the diffuser and the wheels. Separation of the air behind the rear wheels was reduced and increased the effective area of the diffuser.
- A way of guiding the air flow and shield the diffuser from the turbulent air flow from the wheels was to introduce *guiding vanes*. The placement of these vanes are critical in order to achieve a lower drag which could be observed when the implementation resulted in a drag increase. This rise in drag originates from the fact that the stagnation pressure in the front had moved and increased in magnitude. A concluding remark could be done on how the air flows onto the vanes which resulted in an induced drag due to a non symmetric flow which altered the conditions under the vehicle. This change in e.g. pressure under the vehicle increased the stagnation pressure and thereby the pressure difference between the front and rear hence a high pressure drag.
- Due to large fluctuations in the flow field around the radiator no real conclusive remark can be made.
- Implementation of *vortex generators* had the intended function to delay separation and disturb the flow in a positive way which was successful in the case where a 5° diffuser was used on the *SAAB 9-3 Sports wagon* model. The induced vortices created by the vortex generators (VGs)

interacted with the turbulent flow from the rear wheels in favorable way. How this interaction in detail work is not establish since the improvement is slight and the forces analysis gave no indicating in which area an large alteration in flow behavior could be noted.

- A change in the air motion in the wake has been noted by the vector images presented in previous sections that will in some cases cause dirt accumulation in the rear window.
- A major conclusion of this master thesis is that the diffuser has a very general affect on the entire flow field which means that the diffuser has slightly positive impact in terms of drag reduction on the entire vehicle instead of a specific region.
- An investigation of the actual fuel reduction was preformed at SAAB which only showed a small decrease in fuel consumption due to the low average speed of the *New European Driving Cycle* (NEDC). But benefits of aerodynmanic improvments will be more prominent at higher drivning speeds which will result in a significantly lower fuel consumption. At higher velocities the aerodynamic drag force is the dominating resisting force and a C_d reduction of 19% will have a prominent effect on the fuel consumption when traveling on e.g. highways.

It should be noted that this study shows possible improvements by geometrically altering the underbody but there is still unresolved issues that require further development.

5.1 Recommendations

To verify all the simulated results from the computer models more realistic conditions must be used that could be achieved by preforming physical wind tunnel tests. A verification of the results can also be done by preforming an asymptotic solution. This means that the same case should be simulated using a different sized computational grid and different turbulence models e.g. $k-\omega$ or *LES*. If the results do not differ between the different setup of the same case an asymptotic solution is achieved.

A major influence on the outcoming results is the direction the air travels onto the vehicle, so called the winds yaw angle (z-axis rotation). In this study the yaw angle is set to 0° but an investigation of how cross-winds affects the modifications done ton the underbody can lead to a total redesign of the proposed design form this master thesis.

Thermal attributes like heat transfer from the exhaust system must be controlled to avoid high temperatures in sensitive regions which has not been simulated. Areas where high temperatures are possible due to the geometric modifications proposed are the brakes when covering the wheels and regions on the undercarriage when introducing plates. Another area that should be investigated further is the change in cooling flow trough the engine bay which has been done but only briefly. This investigation can be preformed by sealing of the radiator and comparing the result to reach any new conclusions.

As the vehicles becomes more high-tech and sophisticated new demands has been introduced in the area of automotive aerodynamics such as dirt on sensors for example. This aspect of aerodynamics must be investigated on the proposed solution which can be done in physical wind tunnel testing. Under conditions that exits e.g. in Sweden the undercarriage must be designed to avoid areas where ice and snow can be accumulate.

The field of aerodynamics is highly driven by the constant demand of more fuel efficient vehicle which also means that any new part that goes on the vehicle must be optimized for low weight. This means that an weight optimization on the diffuser and panels must be done that can result in discarding

unnecessary surfaces. The material of which the diffuser and panels will be manufactured of should be light-weight but also meet demands on cost, recycling and manufacturing process.

To be able to embrace the proposed design of the underbody a new exhaust muffler must be developed that can be integrated under the diffuser. The current placement of the spare-wheel must also be relocated in order to achieve a drag reduction by implementing a diffuser.

Today *SAAB Automobile* assembly vehicle according to the line production principle which sets demands on the how parts are designed in order to assemble part easy and quick. An adjustment of the diffuser design due to fit the assembly line can lead to new CFD simulations.

To capture how the flow field changes over a time period a transient simulation should be done and resolve issues of fluctuating flow.

A flat underbody can lead to complications in terms of *noise, vibration* and *harshness* (NVH) which has to be investigated to meet requirements of ride comfort.

The simulation of the radiator may require a transient simulation due to the large differences between the different steady state simulations. Or the radiator can modeled as a porous medium for more accurate results.

References

[1] ANSYS. *Fluent 6.3 User's Guide*. Fluent Inc., 2009.

[2] R. H. Barnard. *Road Vehicle Aerodynamic Design An Introduction Third Edition*. MechAero, 2009.

[3] L. Davidsson. *An Introduction to Turbulence Models*. Department of Thermo and Fluid Dynamics Chalmers University of Technology, 2003.

[4] W. Malalasekera H. K. Versteeg. *An introduction to Computational Fluid Dynamics- The Finite Volume Method*. Pearson Education Limited, 2007.

[5] Wolf-Heinrich Hucho, editor. *Aerodynamics of Road Vehicles Fourth Edition*. SAE International, 1998.

[6] Angle Huminic Gabriela Huminic. Computational study of flow in the underbody diffuser for a simplified car model. 2010.

[7] G. Dutil J. Syms G. Sovran Kevin R. Cooper, T. Bertenyi. The aerodynamic perfoemance of automotive underbody diffuser. 1998.

[8] O. Lögdberg. Turbulent boundary layer separation and control. 2008.

[9] N. Hamamoto M. Koike, T. Nagayoshi. Reserach on aerodynamic drag reduction by vortex generator, mitsubishi motors. 2004.

[10] Jesper Marklund. Minimize vortex drag of a passenger car. 2010.

[11] S. McBeath. *Competition car Downforce*. Haynes Publishing, 1998.

[12] S. McBeath. *Competition car Aerodynamics*. Haynes Publishing, 2006.

[13] C. D. Scott-Pomerantz. *The K-Epsilon Model in the Theory of Turbulance*. Doctoral Thesis, 2004.

[14] Frank M. White. *Fluid mechanics Sixth Edition*. McGraw-Hill International Edition, 2008.

[15] L. Löfdahl L. Josefsson Z. Qiu, C. Landström. Wheel aerodynamic developments on passenger cars by module-based prototype rims and stationary rim shields. 2010.

A Appendix; Additional figures and tables

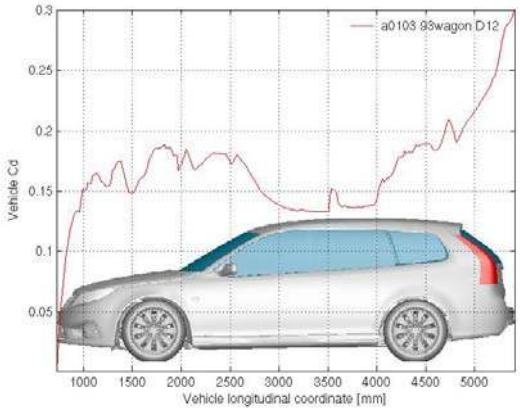

Figure 74: Accumulated drag Wagon, *W3*

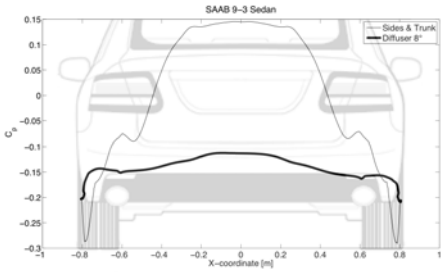

Figure 75: C_p in x=*5.0* on the 8° diffuser, *Sedan*

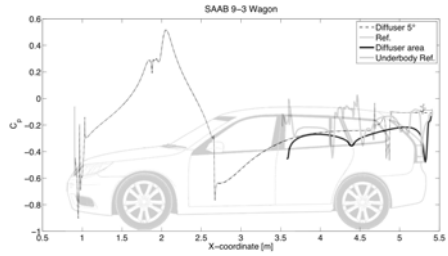

Figure 76: C_p plot in symmetry plane (y=*0*) *SAAB 9-3 Sport wagon*

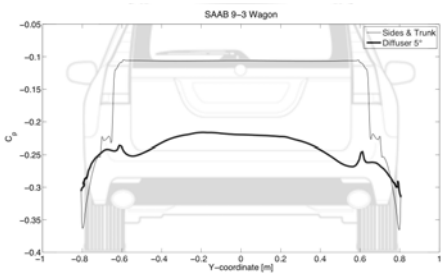

Figure 77: C_p surface tracing at fix location of x=*5.0* m, *Wagon*

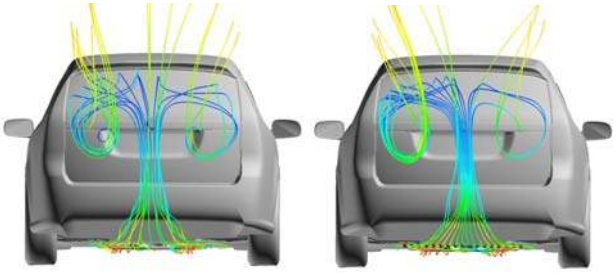

(a) With vortex generators (b) Without vortex generators

Figure 78: Streamlines indicating the upwash from behind

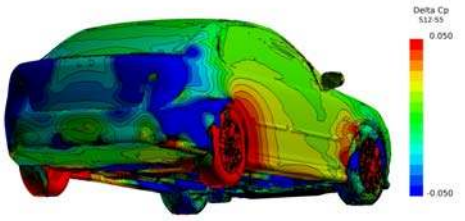

Figure 79: Pressure coefficient difference between *S12-S5*

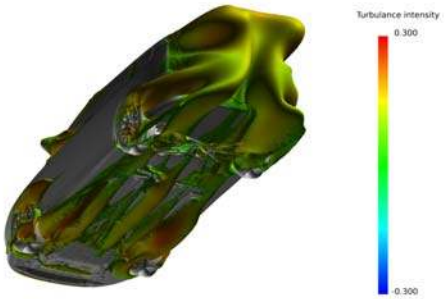

Figure 80: *Iso*-surfaces without the cover panels, just the diffuser, *W15*

B Appendix; Drawings

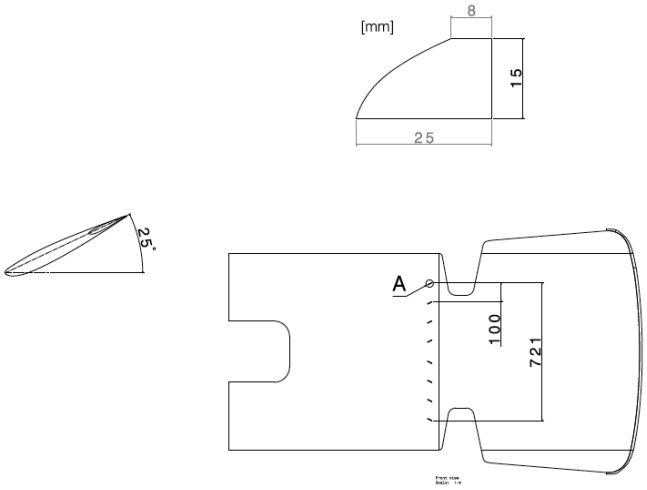

Figure 81: Vortex generators

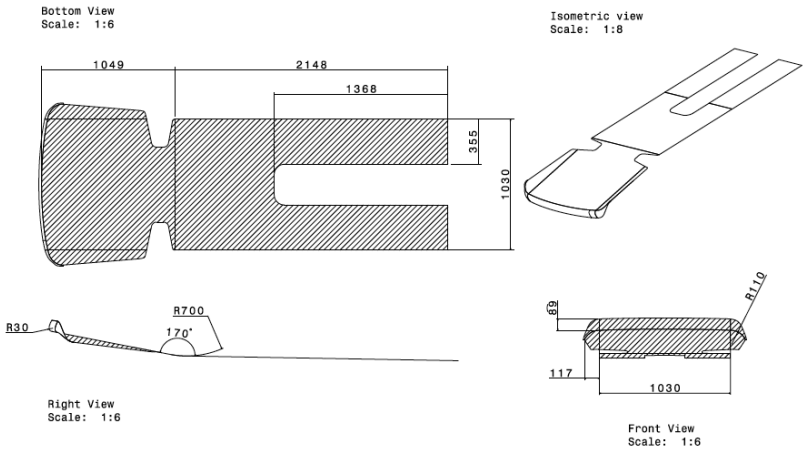

Figure 82: Diffuser, 10°

C Appendix; Journal-file FLUENT

```
;;Read file
/file/rc 9-3wagon_volmesh_u.cas

;;Scale
/mesh/scale 0.001 0.001 0.001

;;Mesh-interface
/define/mesh-interfaces/create prism-interface prism-side-6 ()
        prism-side-6-intf:3048 () n n

;;Turbmodel
/define/models/viscous/ke-realizable yes
/define/models/viscous/near-wall-treatment/non-equilibrium-wall-fn yes

;;Reference pressure
/define/operating-conditions/reference-pressure-location -10000 0 5000

;;Cell zone condition
/define/boundary-conditions/fluid/mrf-rear-fluid n n n y -1 n 123.186
        n 0 n 0 n 0 n 4.402906 n 0 n 0.3157015 n 0 n -1 n 0 "none" n n n n
/define/boundary-conditions/fluid/mrf-front-fluid n n n y -1 n 123.186
        n 0 n 0 n 0 n 1.726906 n 0 n 0.3157014 n 0 n -1 n 0 "none" n n n n

;;Boundary conditions
;;domain
/define/boundary-conditions/zone-type/wall-side symmetry
/define/boundary-conditions/zone-type/wall-roof symmetry
/define/boundary-conditions/wall/w-ground y motion-bc-moving
        n n n 38.89 1 0 0 n n 0 n 0.5
/define/boundary-conditions/zone-type/wall-inlet velocity-inlet
/define/boundary-conditions/velocity-inlet/wall-inlet n n y y n
        38.89 n 0 n y 0.1 0.01
/define/boundary-conditions/zone-type/wall-outlet pressure-outlet
/define/boundary-conditions/pressure-outlet/wall-outlet
        n 0 n y n y 0.1 0.01 n n n

;;wheels
;;Front
/define/boundary-conditions/wall/u-wheel-front-left y motion-bc-moving
        n n y n n 0 n 0.5 123.186 1.726906 0 0.3157014 0 -1 0
/define/boundary-conditions/wall/u-wheel-front-mrf y motion-bc-moving
        n n y n n 0 n 0.5 123.186 1.726906 0 0.3157014 0 -1 0
/define/boundary-conditions/wall/u-wheel-front-steelrim-mrf y
        motion-bc-moving n n y n n 0 n 0.5 123.186 1.726906 0 0.3157014
```

```
        0 -1 0
/define/boundary-conditions/wall/u-wheel-front-cover-mrf y
        motion-bc-moving n n y n n 0 n 0.5 123.186 1.726906 0 0.3157014
        0 -1 0
/define/boundary-conditions/wall/u-wheel-front-cover-mrf-shadow y
        motion-bc-moving n n y n n 0 n 0.5 123.186 1.726906 0 0.3157014
        0 -1 0

;;Rear
/define/boundary-conditions/wall/u-wheel-rear-left y motion-bc-moving
        n n y n n 0 n 0.5 123.186 4.402906 0 0.3157015 0 -1 0
/define/boundary-conditions/wall/u-wheel-rear-mrf y motion-bc-moving
        n n y n n 0 n 0.5 123.186 4.402906 0 0.3157015 0 -1 0
/define/boundary-conditions/wall/u-wheel-rear-steelrim-mrf y
        motion-bc-moving n n y n n 0 n 0.5 123.186 4.402906 0 0.3157015
        0 -1 0
/define/boundary-conditions/wall/u-wheel-rear-cover-mrf y
        motion-bc-moving n n y n n 0 n 0.5 123.186 4.402906 0 0.3157015
        0 -1 0
/define/boundary-conditions/wall/u-wheel-rear-cover-mrf-shadow y
        motion-bc-moving n n y n n 0 n 0.5 123.186 4.402906 0 0.3157015
        0 -1 0

;;fanytor
/define/boundary-conditions/zone-type/prism-cap-25 fan
/define/boundary-conditions/zone-type/i-baloons fan
/define/boundary-conditions/zone-type/i-mirror fan
/define/boundary-conditions/zone-type/i-windsh fan
/define/boundary-conditions/zone-type/i-baloons_411 fan
/define/boundary-conditions/zone-type/u-i-wheel-front-cap-mrf fan
/define/boundary-conditions/zone-type/u-i-wheel-front-mrf fan
/define/boundary-conditions/zone-type/u-i-wheel-rear-cap-mrf fan
/define/boundary-conditions/zone-type/u-i-wheel-rear-mrf fan

;;fanytor -tet
/define/boundary-conditions/zone-type/e-u-i-air-duct-ctrl-surf-tet fan
/define/boundary-conditions/zone-type/
        e-u-i-grille_upper_ctrl_surf-tet fan

;;kylare
/define/boundary-conditions/zone-type/u-i-crfm-in-1 fan
/define/boundary-conditions/zone-type/u-i-crfm-in-2 fan
/define/boundary-conditions/zone-type/u-i-crfm-in-3 fan
/define/boundary-conditions/zone-type/u-i-crfm-in-4 fan
/define/boundary-conditions/zone-type/u-i-crfm-in-5 fan
/define/boundary-conditions/zone-type/u-i-crfm-in-6 fan
```

```
/define/boundary-conditions/zone-type/u-i-crfm-in-7 fan
/define/boundary-conditions/zone-type/u-i-crfm-in-8 fan
/define/boundary-conditions/zone-type/u-i-crfm-in-9 fan
/define/boundary-conditions/zone-type/u-i-crfm-in-10 fan
/define/boundary-conditions/zone-type/u-i-crfm-in-11 fan
/define/boundary-conditions/zone-type/u-i-crfm-in-12 fan

;;Reference values
/report/reference-values/area 2.186 ;;(adjuste after)
/report/reference-values/length 4.63
/report/reference-values/velocity 38.89

;;control
/solve/set/under-relaxation/k 0.7
/solve/set/under-relaxation/epsilon 0.7
/solve/set/under-relaxation/turb-viscosity 0.95

;;Monitors
/solve/monitors/force/drag-coefficient y e-* u-* k-* diffuser*
        () y y "cd-history" y 2 n 1 0 0
/solve/monitors/force/lift-coefficient y e-* u-* k-* diffuser*
        () y y "cl-history" y 3 n 0 0 1
/solve/monitors/force/moment-coefficient y e-* u-* k-* diffuser*
        () y y "cm-history" y 4 n 3.058 0 0.384 0 1 0
/solve/monitors/residual/check-convergence n n n n n n
/solve/monitors/surface/set-monitor mass-flow-radiator "Mass Flow Rate"
        u-i-crfm-in-1 u-i-crfm-in-2 u-i-crfm-in-3 u-i-crfm-in-4
        u-i-crfm-in-5 u-i-crfm-in-6 u-i-crfm-in-7 u-i-crfm-in-8
        u-i-crfm-in-9 u-i-crfm-in-10 u-i-crfm-in-11 u-i-crfm-in-12
        ()y 5 y y "Mass-flow-rate-radiator" 1

;;Flow scheme 1st order
/solve/set/p-v-coupling 20 /solve/set/discretization-scheme/mom 0
/solve/set/discretization-scheme/k 0 /solve/set/
        discretization-scheme/epsilon 0

;;Initialize
/solve/initialize/compute-defaults all-zones
/solve/initialize/set-defaults/x-velocity 15
/solve/initialize/initialize-flow

;;FMG
/solve/initialize/fmg-initialization y

;;Run
/solve/iterate 500
```

```
;;2nd order
/solve/set/discretization-scheme/mom 1
/solve/set/discretization-scheme/k 1
/solve/set/discretization-scheme/epsilon 1

;;Run
/solve/iterate 2500

;;Possible additions
/report/forces/wall-forces y 1 0 0 y "x-forces"
/report/forces/wall-forces y 0 0 1 y "z-forces"

;;Save case and data
/file/wcd 9-3wagon-ref2.cas.gz

;;Epxort fieldview
/file/export/fieldview-unstruct 9-3wagon-ref2
pressure
total-pressure vel-magnitude
x-velocity
y-velocity
z-velocity
vorticity-mag
turb-kinetic-energy
turb-diss-rate
y-plus
wall-shear
turb-intensity ()
```